KINETIC AND THERMODYNAMIC CONTRIBUTIONS TO AN INTERMOLECULAR MECHANISM OF SUBUNIT COMMUNICATION: COORDINATION OF PYRUVATE CARBOXYLASE ACTIVITY AMONG SPATIALLY DISTINCT ACTIVE SITES

by

Lauren Westerhold

June, 2016

Director of Thesis: Tonya Zeczycki, Ph.D.

Major Department: Biochemistry and Molecular Biology

Catalysis occurring in a multifunctional enzyme at spatially and functionally discrete active sites is controlled by an array of factors, including enzyme structure, ligand binding, and productive interaction of substrates to facilitate turnover. Completion of the catalytic cycle partially depends upon the ability of these active sites to communicate with one another, as well as with any allosteric regulatory regions of the enzyme. Such long-range communication typically manifests measurable effects on substrate binding or product release. In the case of pyruvate carboxylase (PC), pyruvate binding to the carboxyl transferase (CT) domain induces translocation of the biotin carboxyl carrier (BCCP) domain and subsequently increases the rate of P_i release in the biotin carboxylase (BC) domain. While the kinetic mechanism and structural arrangement of the PC tetramer have been elucidated, the source of intermolecular signals required to facilitate catalysis between active sites remains unclear. The BC and CT domain active sites necessary to produce one oxaloacetate are located on separate polypeptide chains, while binding of acetyl-CoA, the essential allosteric activator, is required for stimulation of the overall catalytic rate. In metabolic regulatory enzymes such as PC, it is essential to understand not only the overall

mechanism of intersubunit communication, but also the thermodynamic driving forces behind ligand relationships to piece together the amino acid network and subunit domains that are responsible for the dramatic stimulatory response elicited upon binding of acetyl-CoA. Ultimately, this would allow for elucidation of the molecular regulatory mechanism of PC and for development of therapeutic strategies to target the chronic hyperglycemia associated with its uncontrolled activity in Type 2 diabetics.

To address the impact of pyruvate occupancy in the CT domain on behavior of other domains, we generated mixed hybrid tetramers using mutants of the catalytically relevant residues E218 (in the BC domain) and T882 (in the CT domain) to measure pyruvate carboxylation and P_i release activities. Our results, which compared the apparent $K_{a\ pyruvate}$ for pyruvate-stimulated P_i release catalyzed by the T882S:E218A$_{(1:1)}$ hybrid tetramer to that of the wild-type and the T882S homotetramer, were consistent with an intermolecular communication mechanism, whereby pyruvate binding at the E218A CT domain was responsible for inducing translocation of the T882S BCCP domain within the same face of the tetramer. We also determined the thermodynamic-linkage of each ligand of PC, that is, the extent to which the presence of one bound ligand influences enzyme turnover in the presence of variable concentrations of another. The ability of either MgATP or pyruvate to increase the affinity of PC for the other is observed in the presence of acetyl-CoA, while this relationship is entirely lost in its absence. Thus, PC's spatially distinct active sites, even in the presence of the preferred substrates, cannot communicate or coordinate productive catalytic coupling in the absence of the activator. Long-term implications of this proposal include determination of the consequences of imbalanced metabolic flux on the regulatory mechanism and catalytic activity of PC in the liver.

KINETIC AND THERMODYNAMIC CONTRIBUTIONS TO AN INTERMOLECULAR MECHANISM OF SUBUNIT COMMUNICATION: COORDINATION OF PYRUVATE CARBOXYLASE ACTIVITY AMONG SPATIALLY DISTINCT ACTIVE SITES

A Thesis

Presented To the Faculty of the Department of Biochemistry and Molecular Biology

Brody School of Medicine at East Carolina University

In Partial Fulfillment of the Requirements for the Degree

Master of Science in Biomedical Sciences

by

Lauren Westerhold

June, 2016

KINETIC AND THERMODYNAMIC CONTRIBUTIONS TO AN INTERMOLECULAR MECHANISM OF SUBUNIT COMMUNICATION: COORDINATION OF PYRUVATE CARBOXYLASE ACTIVITY AMONG SPATIALLY DISTINCT ACTIVE SITES

by

Lauren Westerhold

APPROVED BY:

DIRECTOR OF THESIS:

_____

Tonya Zeczycki, Ph.D.

COMMITTEE MEMBER: _____

Joseph Chalovich, Ph.D.

COMMITTEE MEMBER: _____

Brian Shewchuk, Ph.D.

COMMITTEE MEMBER: _____

Darrell Neufer, Ph.D.

DIRECTOR OF THE MASTER'S PROGRAM
IN BIOMEDICAL SCIENCES: _____

Richard Franklin, Ph.D.

DEAN OF THE
GRADUATE SCHOOL: _____

Paul Gemperline, Ph.D.

DEDICATION

To my family – I truly could not have completed this degree, much less started it, without your continual love, encouragement, and support. I love you all and I cannot thank you enough for all you have done and continue to do for me.

To my fiancé, Matt – Thank you for believing in me and my abilities, even when I do not. You challenge me to be better and your support means more to me than you know. I love you and thank you for everything.

To my colleagues, Stephanie and Jessica – Thank you for your constant guidance, advice, and willingness to listen, and for sharing in this experience alongside me. More importantly, though, thank you for becoming two of my dearest friends in the process.

ACKNOWLEDGEMENTS

I would like to thank Dr. Tonya Zeczycki for the opportunity to complete both this research project and my degree as a member of her laboratory. Her guidance, mentorship, and constant support have been invaluable in my development thus far as a scientist, and the opportunity to work with and learn from her for the past two years has been an immense privilege. I would also like to thank Dr. Joseph Chalovich, Dr. Brian Shewchuk, and Dr. Darrell Neufer for the generous donation of their time, insights, and support as members of my thesis committee.

Additionally, I would like to thank the Brody School of Medicine at East Carolina University and the East Carolina Diabetes and Obesity Institute for offering me the position to study here, as well as for providing the resources and the facilities with which to complete both my degree coursework and my graduate research. Finally, many thanks to the Brody School of Medicine SEED Grant Program, the Office of Sponsored Programs, and the Office of Research and Graduate Studies for providing the funding support necessary to complete this project.

TABLE OF CONTENTS

LIST OF TABLES

LIST OF FIGURES

LIST OF SYMBOLS AND FIGURES

PC	Pyruvate Carboxylase
*Re*PC	PC from *Rhizobium etli*
*Sa*PC	PC from *Staphylococcus aureus*
BC	Biotin carboxylase domain
CT	Carboxyltransferase domain
BCCP	Biotin carboxyl carrier protein domain
HT	Hybrid tetramer
WT	Wild-type form of enzyme
T882S	Serine mutation of residue Thr882 in *Re*PC
E218A	Alanine mutation of residue Glu218 in *Re*PC
ATP	Adenosine triphosphate
ADP	Adenosine diphosphate
P_i	Inorganic phosphate
HCO_3^-	Bicarbonate
Mg^{2+}	Magnesium cation
MDH	Malate dehydrogenase
PNP	Purine nucleoside phosphorylase
MESG	7-methyl-6-thioguanosine
OAA	Oxaloacetate
NADH	Nicotinamide adenine dinucleotide, reduced form
NAD^+	Nicotinamide adenine dinucleotide, oxidized form
MgATP	Magnesium-adenosine triphosphate

FPLC	Fast protein liquid chromatography
Ni^{2+}	Nickel(II) cation
IMAC	Immobilized metal ion affinity chromatography
NTA	Nitrilotriacetic acid
CV	Column volume
EtOH	Ethanol
DMSO	Dimethyl sulfoxide
BME	β-mercaptoethanol
TEMED	Tetramethylethylenediamine
APS	Ammonium persulfate
SDS	Sodium dodecylsulfate
PAGE	Polyacrylamide gel electrophoresis
HEPES	2-[4-(2-hydroxyethyl)piperazin-1-yl]ethanesulfonic acid
EDTA	Ethylenediaminetetraacetic acid
NaCl	Sodium chloride
IPTG	Isopropyl β-D-1-thiogalactopyranoside
$MgCl_2$	Magnesium chloride
TCEP	Tris(2-carboxyethyl)phosphine
NaN_3	Sodium azide
BMOE	Bismaleimidoethane
BMH	Bismaleimidohexane
DTT	Dithiothreitol
Bis-Tris	Bis-Tris methane; buffering agent

V_{max}	Maximum achievable reaction velocity
K_m	Michaelis constant
K_d	Dissociation constant
k_{cat}	Turnover number
PCR	Polymerase chain reaction
DNA	Deoxyribonucleic acid
RNA	Ribonucleic acid
Pfu	RNA polymerase
dNTP	Deoxynucleotide solution mix
DpnI	DNA restriction endonuclease

INTRODUCTION

Enzyme Structure and Function. Pyruvate carboxylase (PC) is a biotin-dependent enzyme that is responsible for the MgATP-dependent conversion of pyruvate to oxaloacetate in the presence of the essential allosteric activator, acetyl-CoA, in a variety of tissues throughout the body (**Fig. 1**) (1, 2). PC is a critical anaplerotic enzyme in glucose metabolism, serving to replenish oxaloacetate consumed by the TCA cycle (1, 3). Previous crystallographic studies identified four distinct domains contained within the PC monomer, namely the biotin carboxylase (BC), biotin carboxyl carrier (BCCP), carboxyl transferase (CT), and allosteric domains. Each domain has been functionally characterized *via* steady-state kinetics and site-directed mutagenic studies of catalytically relevant residues (4-7). PC is found in a variety of species in both $\alpha_4\beta_4$ and α_4 forms, though $\alpha_4\beta_4$ PCs are primarily found in archaea and some bacteria. In α_4 PCs, such as those found in *Rhizobium etli* and *Staphylococcus aureus*, all functional domains are contained on a single ~130 kDa molecular weight polypeptide chain and the overall tetrameric arrangement of the holoenzyme creates two catalytic faces (**Fig. 2**) (2, 8). This tetramer is a dimer of dimers, in which each face is composed of a dimer of monomers arranged antiparallel to one another (8).

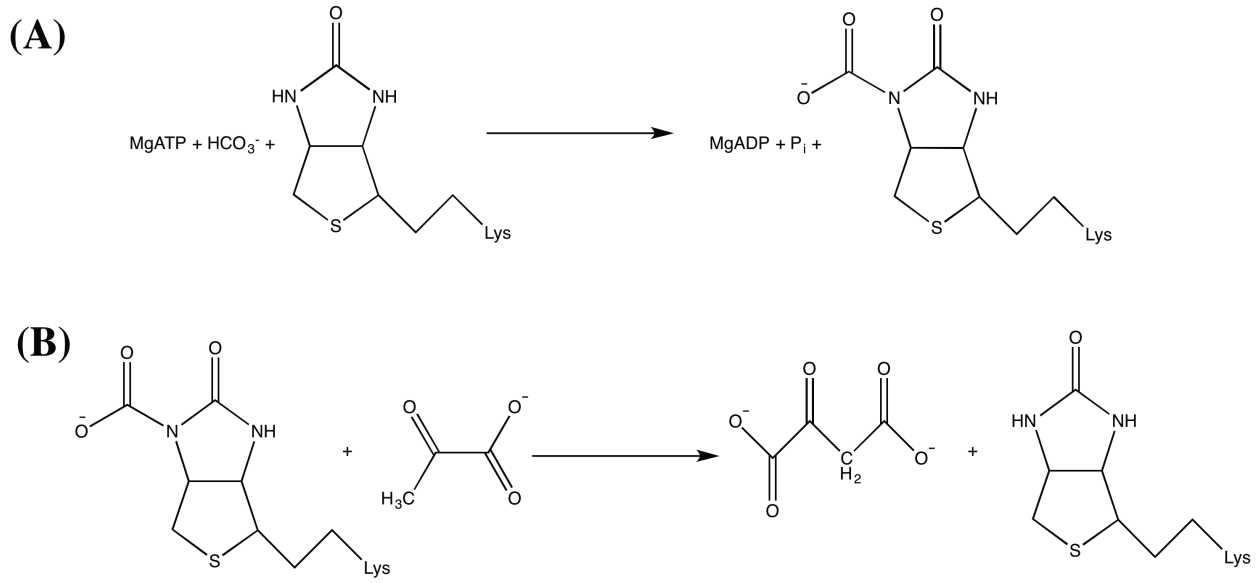

FIGURE 1. Pyruvate carboxylation occurs in a two-step mechanism at two spatially distinct active sites. The first step (*A*), which takes place in the BC domain, involves carboxylation of the ureido ring on BCCP-tethered biotin, which is ATP-dependent and uses bicarbonate (HCO_3^-) as the CO_2 donor. At this point, the carboxybiotin intermediate has been formed, and the BCCP domain moves away from the BC domain. The second step (*B*) occurs in the CT domain active site upon BCCP translocation. The carboxybiotin intermediate serves as the CO_2 donor, and is then decarboxylated in order to carboxylate pyruvate and produce oxaloacetate. Figure generated using ChemDraw Professional (v15.0.0, Perkin Elmer).

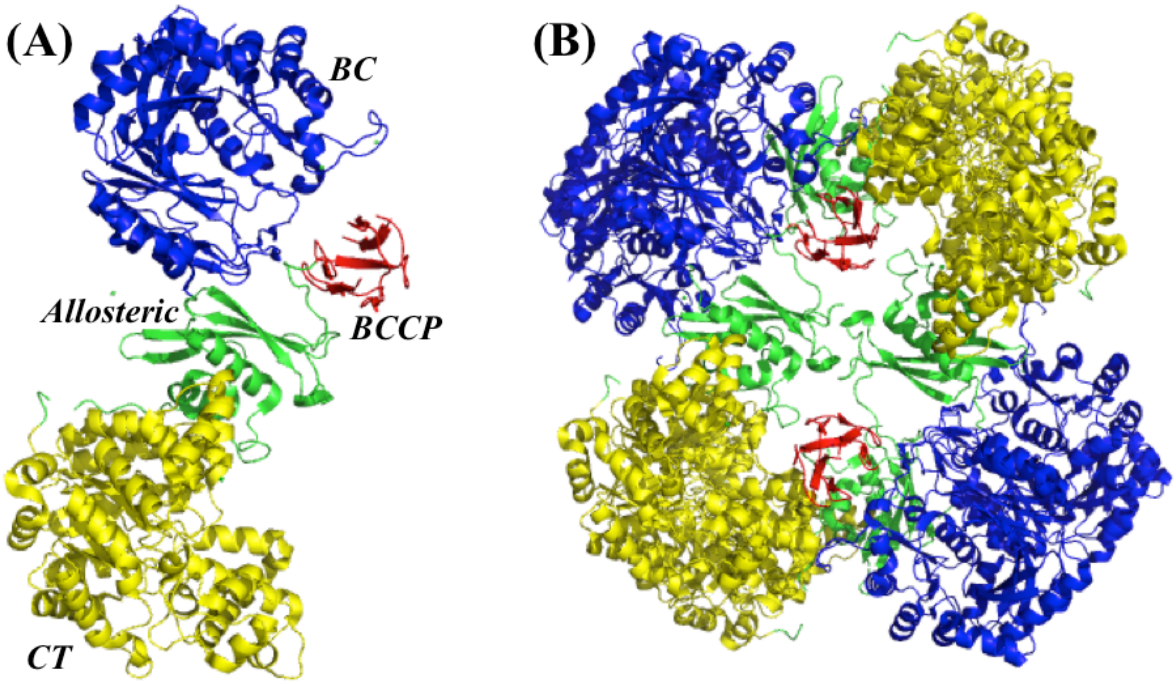

FIGURE 2. Crystal structure of PC (PDB file 2QF7) (8). depicting one single monomer (*A*) and the general tetrameric structure (*B*). Each monomer possesses a biotin carboxylase (BC) domain, an allosteric domain, a carboxyltransferase (CT) domain, and a biotin carboxyl carrier protein (BCCP) domain. BC domains are represented in blue, allosteric domains in green, CT domains in yellow, and BCCP domains in red. The BCCP domain contains a terminal, conserved Lys residue (K1119 in *Re*PC numbering) at which biotin is covalently attached. In the tetrameric structure, the top and bottom faces, each made up of a pair of monomers oriented antiparallel to one another, are arranged perpendicularly to each other, such that significant residue interactions occur between faces at both the BC domains and CT domains. These BC—BC and CT—CT interactions serve to stabilize the tetramer. Catalysis occurs intermolecularly within a single face, whereby the BCCP domain swings between the BC domain of its own polypeptide chain and the CT domain of the opposing polypeptide chain. Structures generated using PyMOL Molecular Graphics System (v1.8, Schrödinger, LLC).

The biotin carboxylase domain, which is the site of MgATP-cleavage and carboxylation of the biotin cofactor by HCO_3^-, is found on the N-terminal end of the PC monomer, and is composed of three distinct sub-domains: the N-terminal A-domain, the B-subdomain lid, and the C-domain (9). The A- and C-domains together make up the substrate binding region of the BC domain, while the B-subdomain rotates to enclose the active site and the disordered, flexible T-loop, which connects two β strands within the B-subdomain, becomes ordered upon ATP binding to facilitate the closing motion of the B-subdomain (9). The biotin moiety of PC is covalently attached to a conserved lysine residue at the C-terminal end of the BCCP domain, and interacts with the BC domain in order to form the carboxylated intermediate. The BCCP domain serves as a flexible linker arm (~ 16 Å in length) that is capable of translocating biotin away from the BC domain on its own polypeptide chain to the CT domain on an opposing polypeptide chain (10). However, given that the distance between the BC domain and the CT domain on an opposing polypeptide within a face averages 55 – 85 Å across biotin-dependent carboxylases such as PC, propionyl-CoA carboxylase (PCC), and 3-methylcrotonyl-CoA carboxylase (MCC), it is possible that the BCCP domain itself must also translocate during catalysis (10-14). The extent to which the BCCP domain actually moves remains unclear, based on recent crystallographic structural studies showing PC isoforms adopting a range of symmetrical and asymmetrical quaternary conformations (14). In a symmetric structure, it is essential to the intermolecular kinetic mechanism that the BCCP domain translocates, as the distance between the BC and CT domain active sites is ~75 Å; however, in an asymmetric structure, the distance between the active sites is significantly different (~65 Å in the top layer as opposed to ~80 Å in the bottom layer), such that the BCCP domain would not necessarily be required to move dramatically in the top face. Until BCCP domain translocation is observed directly, it is not possible to confirm the extent to

which the BCCP domain moves, but evidence from the literature is suggestive of BCCP domain translocation in response to pyruvate binding in the CT domain (11-14).

The BC domain active site contains several catalytically relevant amino acid residues (**Fig. 3, 4**), which are involved in MgATP-cleavage (Glu218 and Lys245), HCO_3^- deprotonation (Glu305 and Arg301), and biotin enolization (Arg353); of these, a catalytic triad is formed between residues Glu218, Lys245, and Glu305, serving to generate a hydrogen-bonded bridging network between the MgATP and HCO_3^- binding pockets within the active site. Glu305 and Lys245 act together to deprotonate HCO_3^-, properly align the terminal γ-phosphate group of MgATP in the binding pocket, and initiate nucleophilic attack on the γ-phosphate by HCO_3^- (6). The position of Glu218 allows for formation of a low barrier hydrogen bond between itself and Glu305, serving to partially stabilize the carboxyphosphate intermediate formed prior to generation of the carboxybiotin intermediate (**Fig. 1, 3**).

Upon formation of the carboxybiotin intermediate in the BC domain, the BCCP domain is precluded from the BC domain active site as a protective mechanism against abortive decarboxylation and uncoupling of ATP hydrolysis from pyruvate carboxylation (5). In order to complete the second half-reaction of pyruvate carboxylation, the carboxybiotin-tethered BCCP domain must translocate a distance of approximately 60 Å between the BC domain of its own polypeptide chain and the CT domain of the opposing polypeptide chain within a face. The carboxybiotin intermediate form of PC is relatively stable in the absence of substrates, but is rapidly decarboxylated in the CT domain upon binding of a CT domain ligand in its active site.

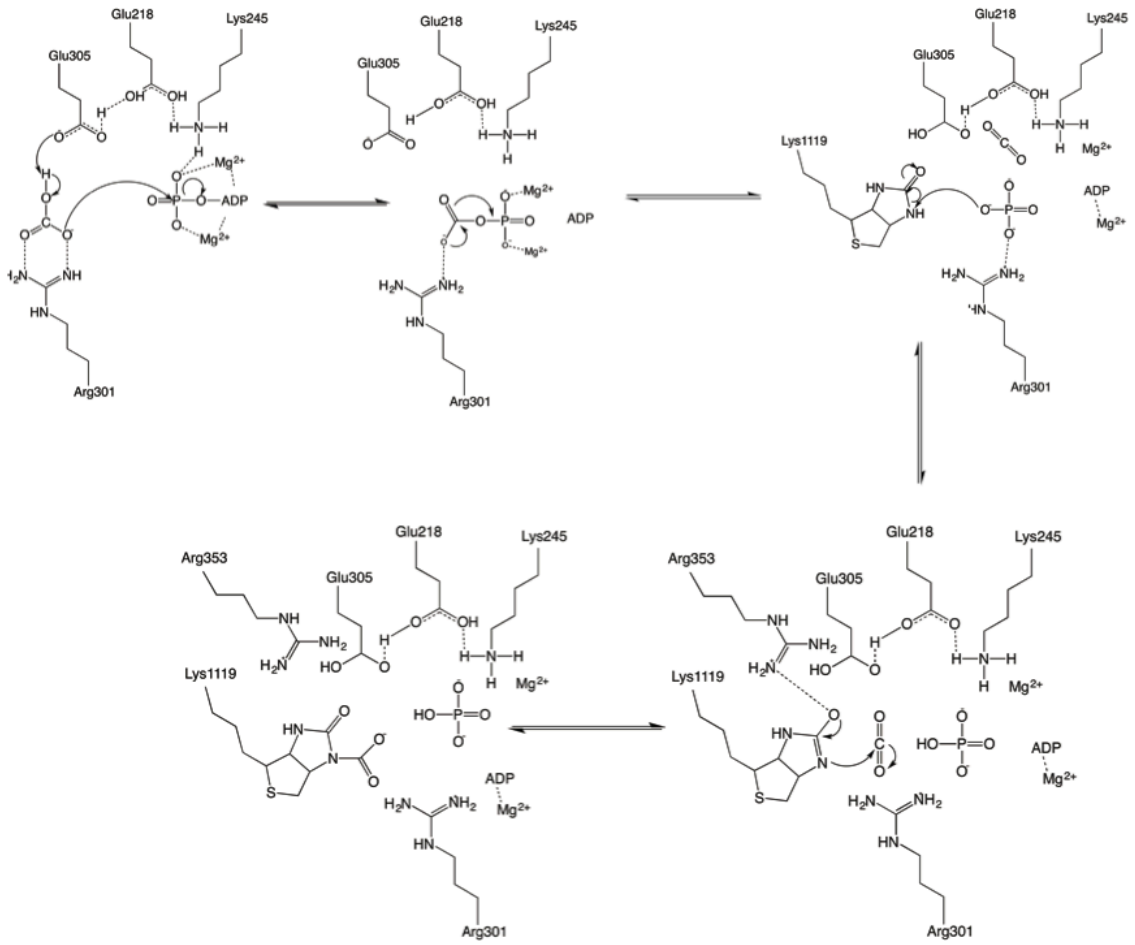

FIGURE 3. The catalytic mechanism of MgATP-cleavage and biotin carboxylation in the BC domain. Adapted from Zeczycki et al., 2011. Figure generated using ChemDraw Professional (v15.0.0, Perkin Elmer).

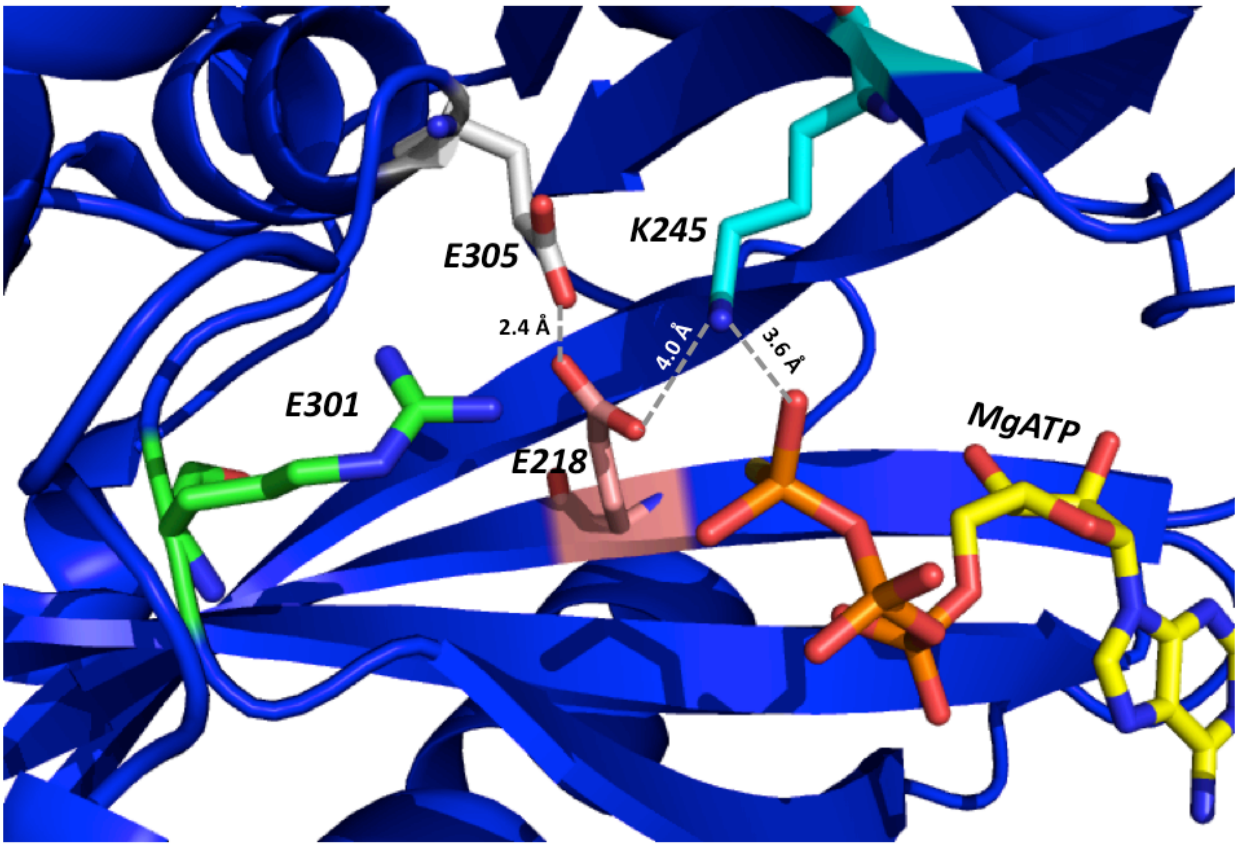

FIGURE 4. The BC domain active site, and catalytically relevant residues therein. Glu218 (pink), Glu305 (white), and Lys245 (blue) comprise the catalytic triad that is required for electrostatic stabilization of MgATP binding in the active site, as well as subsequent hydrolysis and P_i release (shown: ATP-γ-S, a non-hydrolyzable analog of ATP, which was used in crystallization of *Re*PC – PDB ID 2QF7). Arg301 (green) assists Glu305 in deprotonation of HCO_3^-. Structures generated using PyMOL Molecular Graphics System (v1.8, Schrödinger, LLC).

The CT domain active site contains a central $\alpha_8\beta_8$ triose phosphate isomerase (TIM) barrel fold with a long, C-terminal funnel, made up of nine α-helices, leading into the active site (8, 10, 15). A coordinated divalent metal cation is also conserved in the active site to serve as a Lewis acid and stabilize pyruvate binding, enolization, and carboxylation; in *Re*PC and *Sa*PC, this cation is Zn^{2+}. Asp590 and Tyr628 (using residue numbering from *R. etli*) are conserved in the active sites of CT domains found in various forms of PC, as well as in homologous biotin-dependent enzymes. Pyruvate binding in the CT domain causes a conformational change in a flexible loop near the active site, stabilizing the loop and creating a more closed conformation to allow salt bridge formation between the pyruvate carboxyl moiety and the guanidinium group of Arg621 in *Re*PC (5). Tyr628 is particularly notable in terms of its importance for catalysis, creating a sulfur-aromatic interaction between its π-electron cloud and the sulfur atom in the thiophene ring of biotin, thus stabilizing the interaction of biotin with the CT domain (**Fig. 5**).

Several other residues in the CT domain have also been previously identified as being catalytically relevant for the carboxyl group transfer between the tethered carboxybiotin and bound pyruvate (**Fig. 6, 7**). In particular, Arg548 and Gln552 have been proposed to facilitate pyruvate binding in the active site through hydrogen bonding stabilization; the amide group of Gln552 is located only 2.9 Å from the carboxyl oxygen of pyruvate and 3.5 Å from the carbonyl oxygen of pyruvate, while the guanidinyl group of Arg548 also assists in hydrogen bonding with the carbonyl oxygen, offering assistance during enolization (16). Additionally, there is a strictly conserved threonine residue in CT domain active sites across PC forms, numbered Thr882 in the *Re*PC primary sequence, which is critical to completion of the pyruvate carboxylation reaction. Thr882, which has a pK_a of ~13, is protonated at physiological pH, and its hydroxyl group is

arranged such that there is only a 3.9 Å distance between itself and the methyl group of bound pyruvate. This proximity allows Thr882 to act in its essential proton shuttling role, first serving as a general acid in the active site and protonating biotin at its N_1 position following decarboxylation before acting as the general base to abstract a proton from pyruvate and generate the enol-pyruvate intermediate (7, 16). From there, carboxylation can occur and the oxaloacetate product is formed (**Fig. 1, 6**).

Acetyl-CoA, the essential allosteric activator of PC, binds in the allosteric domain located between the BC and CT domains in the primary enzyme structure, specifically in a binding pocket formed between the allosteric and BC domains (**Fig. 8**) (8). Kinetically, its presence has been shown previously to have a significant stimulatory effect on the BC domain reaction, while only slightly affecting the CT domain reaction and resultant oxaloacetate (4). *Re*PC residues Arg427 and Arg472 serve to bind and orient acetyl-CoA in the pocket via interaction with the 3'-phosphate and 5'-α-phosphate, respectively, contributing to the structural stabilization and general allosteric regulation of the enzyme (**Fig. 8**).

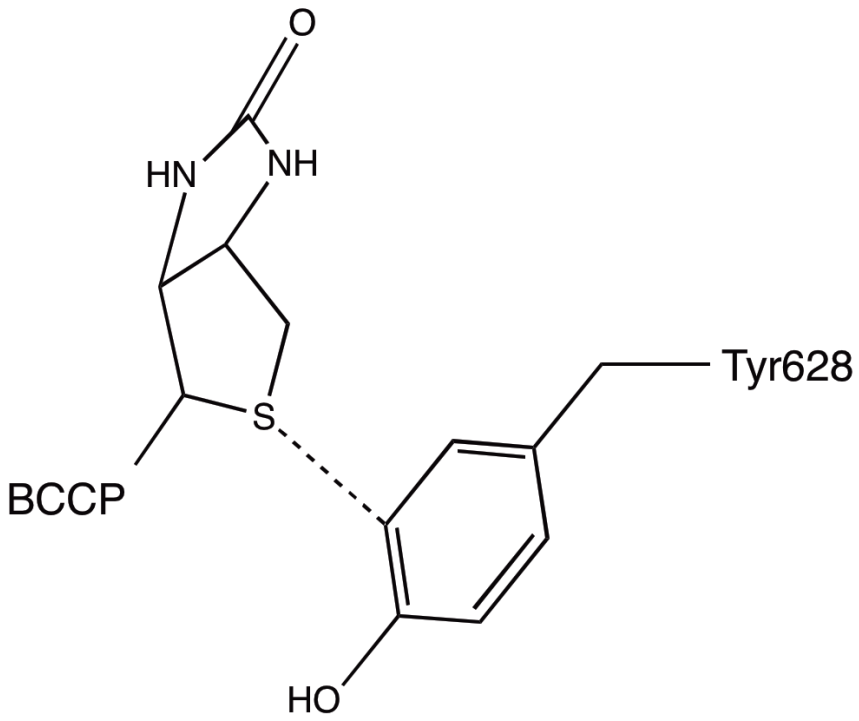

FIGURE 5. Arrangement of the biotin cofactor in the CT domain such that Tyr628 is capable of stabilizing the thiophene ring through interaction with its aromatic π-electron cloud. Figure generated using ChemDraw Professional (v15.0.0, Perkin Elmer).

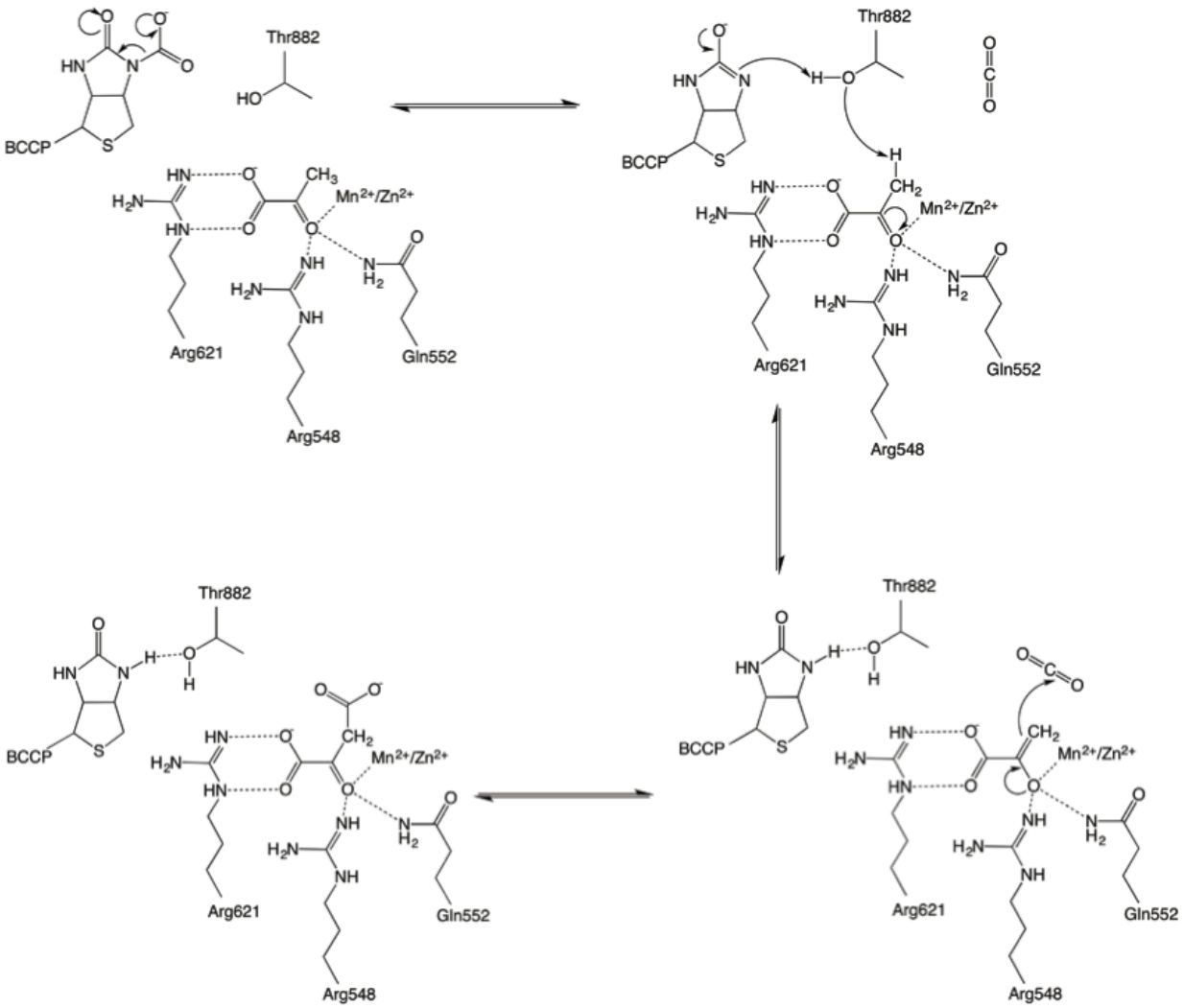

FIGURE 6. Catalytic mechanism of proton shuttling by Thr882 in the CT domain active site to facilitate carboxylation of pyruvate and form oxaloacetate. Adapted from Lietzan and St. Maurice, 2013. Figure generated using ChemDraw Professional (v15.0.0, Perkin Elmer).

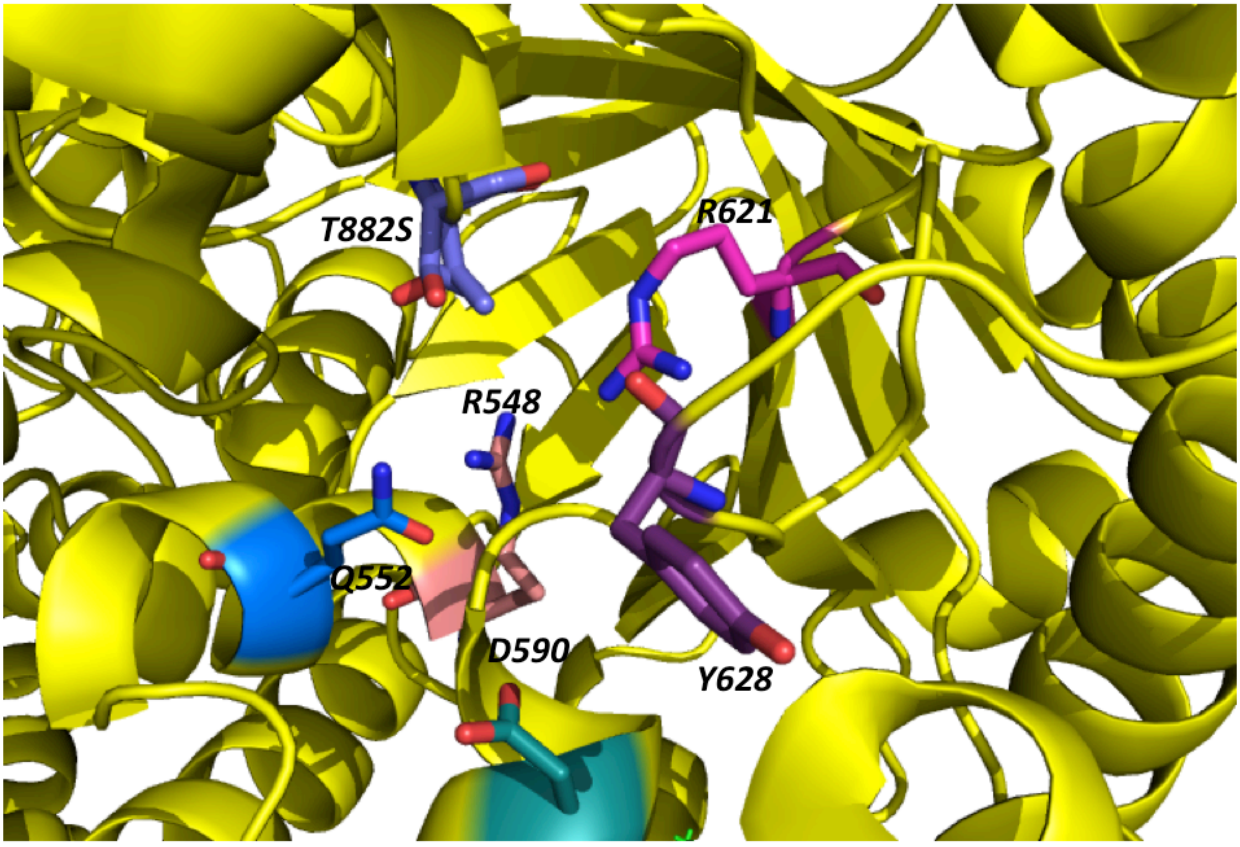

FIGURE 7. In the CT domain active site, Thr882 (light purple) is responsible for proton shuttling within the active site, which is crucial to the transfer of the carboxyl group from the biotin intermediate to pyruvate. Arg621 (magenta), Arg548 (pink), and Gln552 (blue) are responsible for stabilizing pyruvate (not shown) within the active site. Asp590 (teal) and Tyr628 (dark purple) serve to stabilize the carboxylated biotin cofactor upon translocation into the active site. The active site TIM barrel is visible immediately behind the highlighted residues.

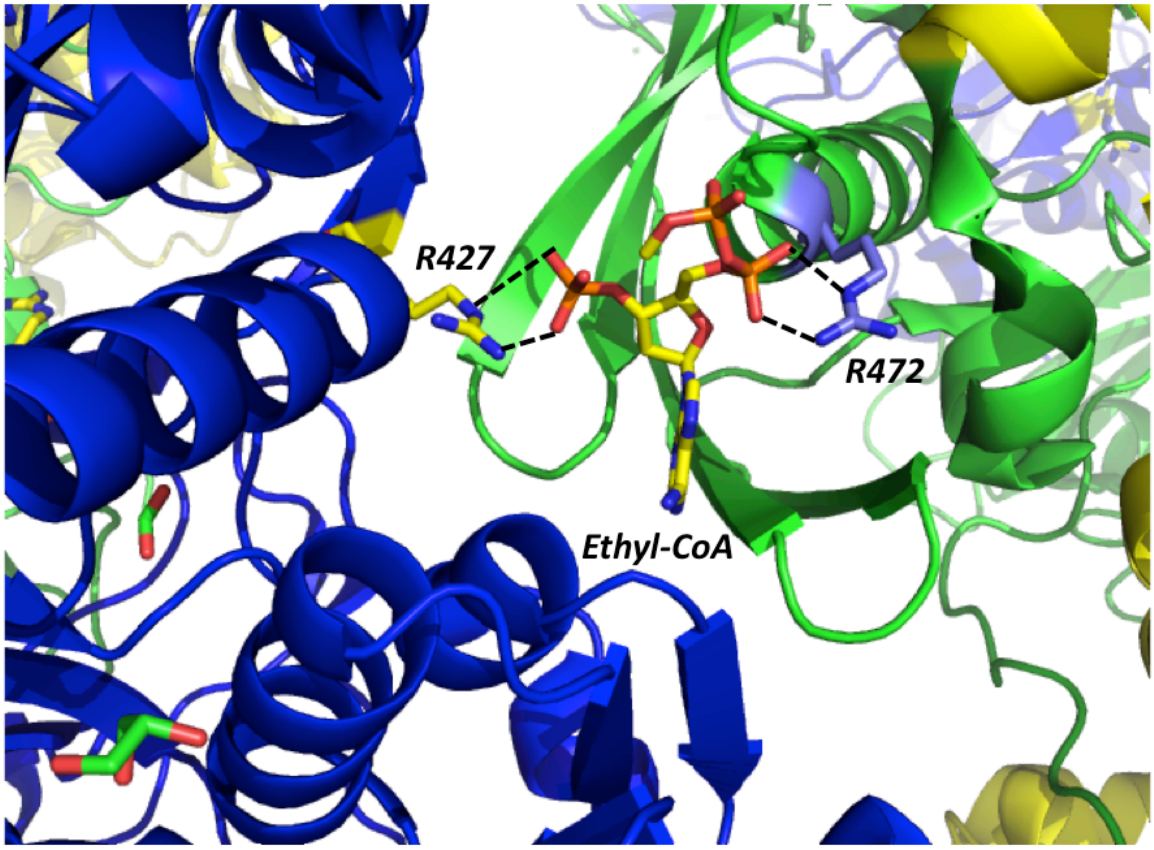

FIGURE 8. Acetyl-CoA binding pocket formed between the allosteric and BC domains. Ethyl-CoA (crystallized with *Re*PC, PDB ID 2QF7). Adapted from Adina-Zada et al., 2012. Structures generated using PyMOL Molecular Graphics System (v1.8, Schrödinger, LLC).

Pathological relevance. Because of its critical role in the regulation of glucose metabolism (**Fig. 9**), aberrant pyruvate carboxylase activity contributes to the pathogenesis of Type 2 Diabetes Mellitus as the major cause of elevated hepatic gluconeogenesis. Insulin resistance due to obesity has been observed in a variety of biological tissues, including skeletal muscle, liver, and white adipose (WAT) (17). In adipose tissue, insulin resistance is manifested as a failure to regulate free fatty acid (FFA) release and subsequent β-oxidation; thus, FFA levels are elevated in diabetic and obese individuals. It is thought that plasma FFA levels, when sufficiently elevated, inhibit insulin-stimulated glucose uptake. This is further supported by the observation that physiological levels of plasma FFAs stimulate secretion of insulin in nondiabetic individuals (18). Ectopic lipid accumulation in the liver and muscle prompts infiltration of macrophages into WAT, resulting in increased rates of lipolysis. Because of this high lipid supply and increased rate of β-oxidation, acetyl-CoA production and release into the plasma is enhanced, thus chronically upregulating hepatic PC activity leading to chronic fasting hyperglycemia and ultimately contributing to the development of obesity-induced insulin resistance (**Fig. 10**) (2, 19).

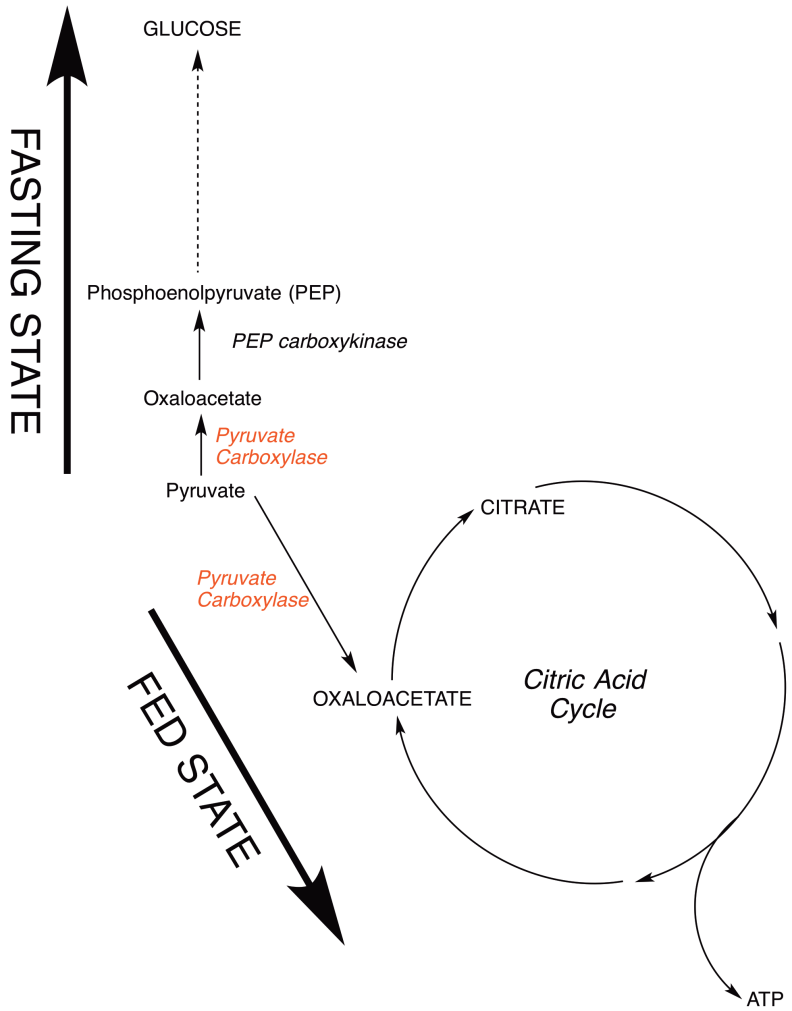

FIGURE 9. Positioning of pyruvate carboxylase in the regulation of glucose metabolism. PC catalyzes the first committed step of the gluconeogenesis pathway, producing oxaloacetate which is then converted to phosphoenolpyruvate (PEP) and eventually to glucose. Gluconeogenesis is upregulated in the fasting state, when plasma glucose levels are relatively low. Alternatively, in the fed state, plasma glucose levels are elevated, which promotes cellular glucose uptake and flux through the glycolytic pathway. In this state, PC serves an anaplerotic role, utilizing pyruvate produced from glycolysis to replenish intermediates of the citric acid cycle, ultimately leading to increased flux through the electron transport chain in the inner mitochondrial membrane and increased ATP production. Figure generated using ChemDraw Professional (v15.0.0, Perkin Elmer).

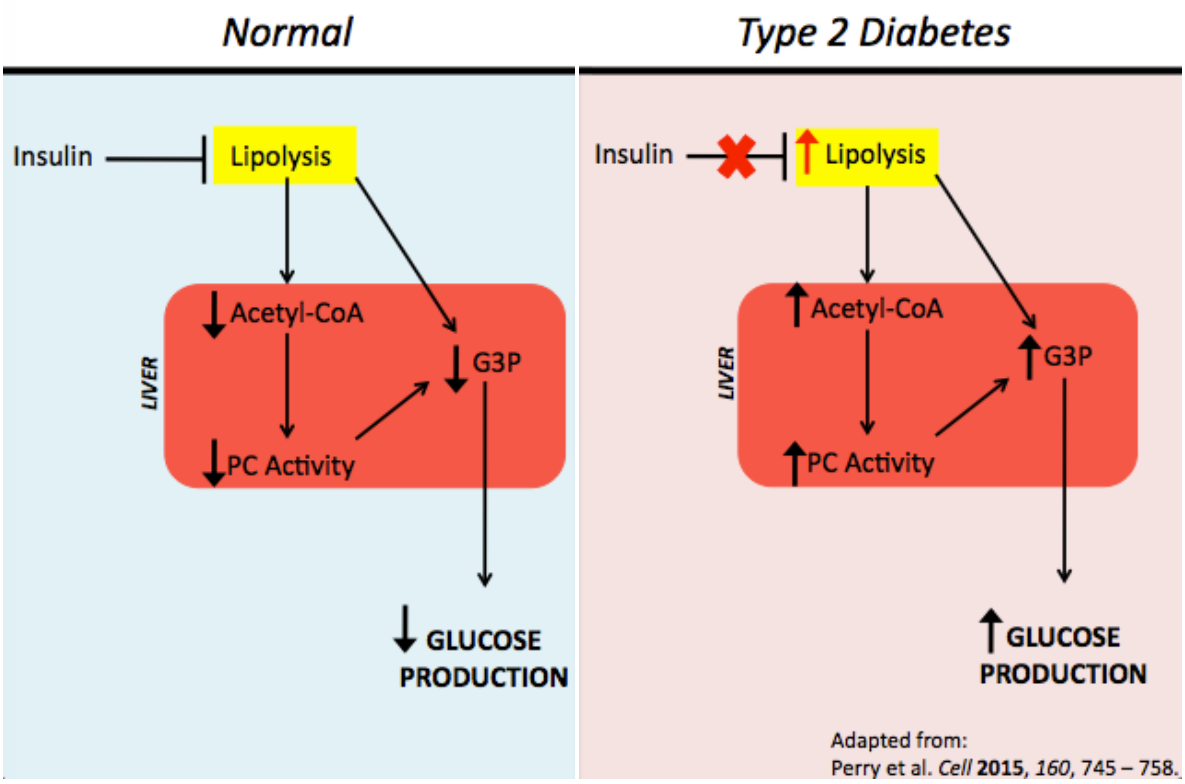

FIGURE 10. PC activity in healthy (*left*) and Type 2 Diabetic (*right*) individuals. Insulin signaling is known to stimulate cellular glucose uptake, as well as to inhibit the rate of lipolysis and β-oxidation occurring in adipose tissue (shown in yellow). Regulation of lipolysis controls the level of acetyl-CoA, the essential allosteric activator of PC, produced from β-oxidation, limiting pyruvate carboxylation activity in the liver (shown in red) and controlling the rate of gluconeogenesis relative to existing plasma glucose concentrations. In the case of Type 2 Diabetes, however, systemic insulin resistance results in the failure of tissues to take up glucose, as well as the inability to regulate the rate of lipolysis occurring in adipose tissue. Persistent upregulation of lipolysis then leads to an elevated concentration of circulating acetyl-CoA, resulting in upregulated pyruvate carboxylation activity and excess production of glucose in hepatocytes. Upregulated PC activity as a result of insulin resistance thus contributes to the persistent fasting hyperglycemia phenotype characteristic of Type 2 Diabetes.

Proposed Research and Hypothesis. While much about the kinetic mechanism of pyruvate carboxylation and the quaternary structural arrangement of monomers has been elucidated, the source of the intermolecular signals required to facilitate catalysis between distinct active sites in this multifunctional, multisubunit enzyme remains unclear. Thus, the primary purpose of this study has been to attempt to gain greater insight into both the kinetic and thermodynamic communication mechanisms coordinating catalytic events in the discrete active sites of PC. Ultimately, we propose that pyruvate occupancy in the CT domain is the primary governing force over BCCP domain translocation within the tetramer, and that the presence of the activator, acetyl-CoA, is required in order for bound pyruvate to elicit its stimulatory effect on the MgATP-cleavage reaction occurring in the BC domain.

Of particular interest to us is the mechanism by which acetyl-CoA regulates and promotes catalysis within the tetramer, and the human body's loss of control over this regulatory mechanism that occurs along with metabolic dysfunction in obese and diabetic individuals. Here, we present insights into the kinetic signaling mechanism of pyruvate carboxylase, which we studied by exploiting PC's tendency to dissociate into monomers when diluted below 2 mg/mL in solution and to rehybridize into functional tetramers in the presence of acetyl-CoA (20). Our results are consistent with an intermolecular signaling mechanism, whereby pyruvate binding in one CT domain induces translocation of the BCCP domain on a *different* polypeptide chain rather than on the *same* polypeptide chain. Additionally, we have examined the extent to which the presence of one ligand (pyruvate, MgATP, or acetyl-CoA) affects the binding and turnover of another to better elucidate the nature of thermodynamic forces underlying allosteric regulation of the enzyme by acetyl-CoA. Taken as a whole, these results are instrumental in our efforts to

define the thermodynamic, kinetic, and structural features of communication pathways within and between subunits in the PC tetramer.

CHAPTER 1 – PYRUVATE OCCUPANCY IN THE CARBOXYL TRANSFERASE DOMAIN OF PYRUVATE CARBOXYLASE FACILITATES PRODUCT RELEASE FROM THE BIOTIN CARBOXYLASE DOMAIN THROUGH AN INTERMOLECULAR MECHANISM

While the kinetic mechanisms for both the BC and CT domains have been well defined in previous studies, the specific mechanisms underlying coordination of catalysis between the two spatially distinct active sites remain unclear. The dependence of catalysis on substrate binding, namely pyruvate occupancy of the CT domain active site, has been established for the release of inorganic phosphate (P_i) upon completion of the HCO_3^- dependent MgATP-cleavage reaction in the BC domain (11, 21, 22). While P_i release is observed in the absence of pyruvate, pyruvate occupancy of the CT domain stimulates translocation of the BCCP domain away from the BC domain and significantly enhances the rate of P_i release. This suggests that the presence of pyruvate in the CT domain initiates some degree of conformational changes or thermodynamically linked binding events that ultimately coordinate the reactions occurring in the BC and CT domains (23).

It has been established that catalysis occurs through an intermolecular mechanism within a single face of PC, whereby the BCCP domain of one polypeptide chain, upon carboxybiotin intermediate formation in the BC domain, is translocated to the active site of the CT domain on the opposing polypeptide chain to carboxylate the bound pyruvate and release oxaloacetate (12-14, 24). However, the method by which CT domain occupancy triggers this translocation and, more specifically, which CT domain within the face communicates with a given BCCP/BC domain has not been addressed. Previous studies have demonstrated that P_i release occurs as a

function of pyruvate occupancy in the CT domain, with the rate rising dramatically in its presence versus its absence. This dependence on pyruvate offers an indirect method by which to measure BCCP domain translocation, as well as to examine the ability of specific CT domain mutants to trigger this same movement.

In order to determine whether BCCP domain movement is controlled by an intramolecular or intermolecular signaling mechanism (that is, whether pyruvate binding on the same polypeptide chain or on the opposing polypeptide chain signals and initiates translocation), we have generated hybrid tetramers (**Fig. 11**) using two specific mutations of catalytically relevant residues (**Fig. 4, 7**). Thr882, which is found in the active site of the CT domain and is known to be essential to proton shuttling between the carboxybiotin intermediate and bound pyruvate, was mutated to Ser and characterized in this study. This mutant exhibits a drastically reduced affinity for pyruvate binding while retaining 3-5% wild-type activity in the CT domain and full wild-type activity in the BC domain. Glu218, a member of the catalytic triad in the MgATP binding pocket of the BC domain, was characterized in a previous study and mutated to Ala, such that BC domain activity was abolished and the CT domain possessed wild-type affinity for pyruvate but reduced activity (**Fig. 11**).

Based on the predicted orientation of the two mutant monomers within a tetramer (**Fig. 11**), we were able to distinguish between intramolecular and intermolecular signaling mechanisms of BCCP translocation through measurement of k_{cat} and $K_{m\ pyruvate}$ for the full-forward pyruvate carboxylation reaction, as well as the apparent $K_{a\ pyruvate}$ for the pyruvate-stimulated P_i release half-reaction. Here, we report initial rates of oxaloacetate formation and P_i release as a function

of increasing concentrations of pyruvate for the PC wild-type, T882S homotetramer, and hybrid tetramers. For the majority of combinations of hybrid tetramers generated, the observed k_{cat} for both pyruvate carboxylation and pyruvate-stimulated P_i release were consistent with predicted values, which confirmed that rehybridization of monomers occurred in a statistically random fashion. Our data suggests an intermolecular signaling mechanism, whereby pyruvate binding in the CT domain influences translocation of the BCCP domain on the opposing polypeptide chain. These results are of high importance in beginning to define the physical and thermodynamic nuances of pyruvate carboxylase communication pathways.

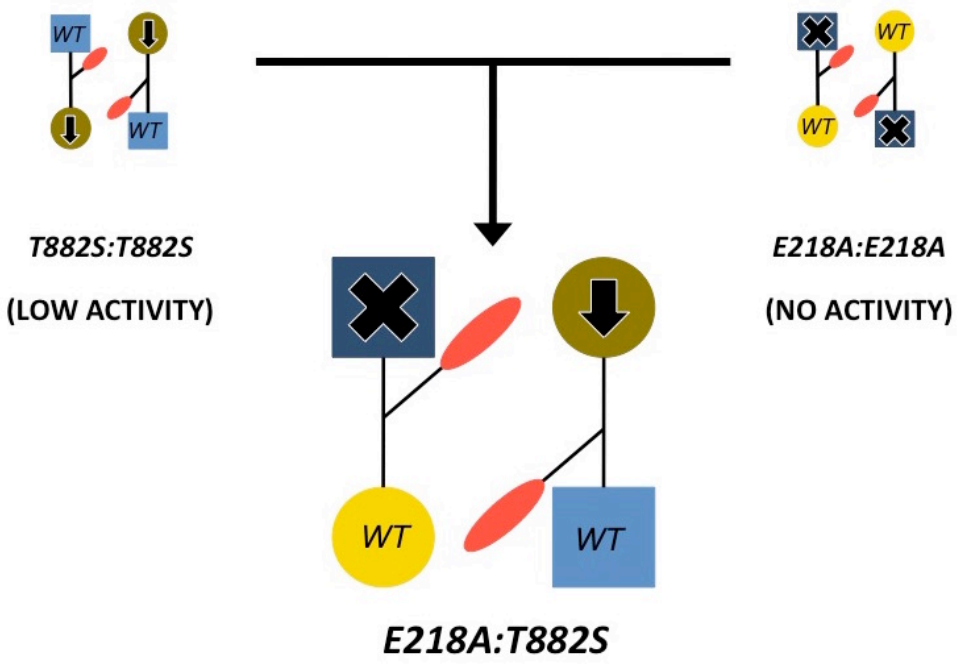

FIGURE 11. Schematic depicting formation of, and orientation of monomers within, *Re*PC hybrid tetramers. In the T882S homotetramer (*top left*), the BC domain with wild-type activity is shown in light blue and the CT domain with dramatically reduced pyruvate affinity is shown in dark yellow. In the E218A homotetramer (*top right*), the defunct BC domain is represented in dark blue, and the CT domain with wild-type pyruvate affinity is in light yellow. Due to the antiparallel orientation of monomers within a single face of PC, the inactive BC domain of E218A and the low-activity CT domain of T882S are paired together, while the functional BC and CT domains are still capable of catalytic turnover (*bottom*).

MATERIALS AND METHODS

Chemicals and Reagents

IPTG, biotin, ampicillin, and chloramphenicol were purchased from Research Products International Corp. (Mt. Prospect, IL). 7-methyl-6-thioguanosine was obtained from Berry and Associates (Dexter, MI). Ni^{2+}-Profinity IMAC resin was obtained from Bio-Rad. Pyruvate sodium salt was obtained from Fisher Scientific. Acetyl-CoA trilithium salt was purchased from Crystal Chem, Inc. (Downers Grove, IL). Malate dehydrogenase was purchased from Calzyme (San Luis Obispo, CA). All other reagents and coupling enzymes were obtained at the highest-grade purity from Sigma-Aldrich and used without further manipulation.

Plasmid Stock Preparation

Electrocompetent *Escherichia coli* TOP10 cells were transformed with the pET-17b plasmid (encoding for *Re*PC) or the pET-28a plasmid (encoding for *Sa*PC) and the pCY216 plasmid (encoding for biotin protein ligase) and incubated in SOC bacterial growth media at 37°C for 1 hour with constant shaking (200 rpm). Transformed cells were plated on LB agar containing ampicillin (for *Re*PC) or kanamycin (for *Sa*PC) and chloramphenicol (for biotin protein ligase) and incubated overnight at 37°C. Individual colonies were selected and used to inoculate 5 mL cultures of LB media supplemented with antibiotics. Inoculated media was incubated at 37°C for 6 – 8 hours with constant shaking (200 rpm). PC plasmids were purified from bacterial lysate using the GeneJET Plasmid Miniprep Kit (Thermo Scientific) and stored at -20°C until use.

Growth and Overexpression of PC

Electrocompetent *E. coli* BL21 Star (DE3) cells were transformed with the pET-17b plasmid or pET-28a plasmid, as well as pCY216. T882S and E218A *Re*PC mutant forms were generated using the QuikChange II XL Site-Directed Mutagenesis Kit protocol (Agilent Technologies).

All PC forms were overexpressed in 12 L cultures of LB media supplemented with 1 mg biotin, ampicillin (100 mg/L final concentration) for *Re*PC or kanamycin (50 mg/L final concentration) for *Sa*PC, and chloramphenicol (35 mg/L final concentration) for plasmid maintenance. The media was inoculated with a 1 L overnight culture of transformed BL21 Star (DE3) cells. Cultures were grown at 37° C with constant shaking (200 rpm) until an OD_{600} of 0.8 – 1.0 was reached. Arabinose (30.5 mM final concentration) was added to the flasks, which were then chilled on ice until an internal temperature of 16° C was reached (~30 min). IPTG (1 mM final concentration) was added, and the flasks were incubated at 16° C for 16 – 20 hr with constant shaking (200 rpm). Bacteria were harvested by centrifugation at 12,000 x g for 20 min. Cell paste was flash-frozen in liquid nitrogen and stored at -80° C. Harvesting yielded a total of 75 – 100 g cell paste per 12 L growth.

Protein Purification Protocol

30 g of cell paste were thawed at 4° C with continuous stirring in 300 mL of lysis buffer containing 20 mM HEPES, 10 mM imidazole, 10 mM $MgCl_2$, 200 mM NaCl, 1 mM TCEP, 200 µg/mL lysozyme, and 1 mM PMSF serine protease inhibitor. Cells were then lysed via sonication (Branson Digital Sonifier, 6 min, max temp 10 °C, 80% amplitude, pulse 59.9 s, pulse off 30 s). All purification steps were performed at 4° C. The lysate was clarified via

centrifugation (12,000 x g for 15 min). The lysate was loaded at 1.5 mL/min onto 25 mL of Profinity^{TM} IMAC Ni^{2+} Charged Resin (Bio-Rad) that was equilibrated with 5 CV of wash buffer containing 20 mM HEPES (pH 8.0), 10 mM $MgCl_2$, 20 mM imidazole, 200 mM NaCl, and 1 mM TCEP. After sufficient washing, the protein was eluted using a 100 mL linear imidazole gradient (10 mM – 300 mM). Fractions containing PC were identified using SDS-PAGE, pooled and dialyzed overnight against 2 L of dialysis buffer (2 x 1 L, 10 mM HEPES, 10 mM $MgCl_2$, 50 mM NaCl, and 1 mM TCEP). The dialyzed protein was then loaded at 1.5 mL/min onto 25 mL of Q Sepharose^{TM} Fast Flow Resin (GE Healthcare) that was equilibrated with 5 CV of wash buffer containing 20 mM HEPES, 10 mM $MgCl_2$, 50 mM NaCl, and 1 mM TCEP. The protein was then eluted using a 100 mL linear NaCl gradient (50 mM – 1 M). Fractions containing PC were identified using SDS-PAGE and dialyzed overnight against 2 L of dialysis buffer (2 x 1 L, 10 mM HEPES, 10 mM $MgCl_2$, 50 mM NaCl, 1 mM TCEP, and 1 mM NaN_3). The purified enzyme was then concentrated to ~ 3 mg/mL using a pressure-based concentration cell (EMD Millipore), flash-frozen in 250 µL aliquots, and stored at -80° C until used. Purity was estimated from SDS-PAGE (>98%) and total protein concentration was determined using a BCA Protein Assay Kit (Pierce).

SDS-PAGE Analysis

Sodium dodecyl sulfate-polyacrylamide gel electrophoresis (SDS-PAGE) was used to visualize purified PC based on molecular weight. SDS gels were composed of a 5% acrylamide stacking buffer (0.5 M Tris-HCl, pH 6.8) and a 9% acrylamide running buffer (1.5 M Tris-HCl, pH 8.8). Protein samples were taken from fractions collected during the elution phase of the purification protocol, mixed in a 1:2 ratio with SDS loading buffer (0.5 M Tris-HCl, pH 6.8; 25% v/v

glycerol; 2% w/v SDS; 0.01% w/v Bromophenol Blue; 5% v/v ß-mercaptoethanol), and boiled on a hot plate at 95°C for 5 min. Boiled samples were loaded into wells in the gel stacking buffer, and current was applied with constant voltage (200 V) for 60 min in SDS running buffer (25 mM Tris base, 0.2 M glycine, 3.5 mM SDS). Electrophoresis was carried out using the Mini-Protean Tetra System (Bio-Rad). Gels were then incubated in Coomassie Blue R-250 protein dye (Bio-Rad) and destained at 4°C overnight before visualization.

Generation of Hybrid Tetramer Forms of RePC

Concentrated wild-type *Re*PC, and T882S and E218A mutant forms of the enzyme were diluted with 100 mM Tricine (pH 7.6) to a final concentration of 1 mg/mL. The diluted enzymes were individually incubated at room temperature for 30 min to allow for complete dissociation of the tetramers.(20) To generate the WT:E218A$_{(1:1)}$ hybrid tetramers, equal volumes of diluted wild-type and the E218A mutant form were combined together at a final concentration of 1 mg/mL (**Fig. 11**). Acetyl-CoA (0.24 mM final concentration) was added in order to promote rehybridization. The protein mixture was then incubated for 30 additional min at room temperature to allow for complete rehybridization into tetramers (13). Similarly, the WT:T882S$_{(1:1)}$, WT:E218A$_{(1:1)}$, and E218A:T882S$_{(1:1)}$ were generated by mixing equal volumes of the diluted wild-type, T882S, and E218A enzyme solutions. The T882S:E218A$_{(4:1)}$ and T882S:E218A$_{(1:4)}$ tetramers were generated by mixing the diluted T882S and E218A enzyme solutions in a 4:1 and 1:4 ratio, respectively. The hybrid enzymes were used without any further purification or manipulation.

Steady-State Enzyme Activity Assays

The initial rates of pyruvate carboxylation and HCO_3^- dependent MgATP-cleavage were determined spectrophotometrically using coupled assay systems. All reactions were performed at 25° C in 1 mL reaction volumes and 100 mM Tricine (pH 7.6). Assays were carried out using the Shimadzu UV-1800 Spectrophotometer, CPS-240A Cell Positioner, and 6 Cell-Thermoelectrical Temperature Controller.

Determination of the Initial Rates of Pyruvate Carboxylation

The ability of the WT, mutant, and hybrid tetramer forms of PC to catalyze the carboxylation of pyruvate was determined using the malate dehydrogenase coupled assay system, monitoring the concomitant oxidation of NADH to NAD^+ at 340 nm (ε_{340} = 6220 M^{-1} cm^{-1}). The initial rates of oxaloacetate formation were measured at variable concentrations of pyruvate (0.25 – 40 mM) and saturating concentrations of all other substrates. Reactions contained: 100 mM HCO_3^-, 2.5 mM MgATP, 2.5 mM $MgCl_2$, 0.25 mM acetyl-CoA, 0.25mM NADH, and malate dehydrogenase (12 units). Reactions were initiated with the addition of ~1.5–800 μg of PC.

Determination of the Initial Rates of P_i Release from the BC Domain

The initial rates of P_i release from the HCO_3^- dependent cleavage of MgATP in the presence of varying concentrations of pyruvate (0 – 40 mM) were determined using the purine nucleoside phosphorylase (PNP) coupled assay system(25, 26) and monitoring the concomitant formation of 2-amino-6-mercapto-7-methylpurine from 7-methyl-6-thioguanosine (MESG) at 360 nm (ε_{360} = 6300 M^{-1} cm^{-1}). Reactions contained: 100 mM HCO_3^-, 2.5 mM MgATP, 5 mM $MgCl_2$, 0.25 mM

acetyl-CoA, 0.2 mM MESG, and purine nucleoside phosphorylase (10 units), and were initiated with ~1.5–350 μg of PC.

Data Analysis

Probability Analysis of Monomer Distribution in Rehybridized Tetramers. We determined the probability of relative distribution of mutant or wild-type monomers for the homogenous population of the WT:E218A$_{(1:1)}$, WT:T882S$_{(1:1)}$, T882S:E218A$_{(1:1)}$, T882S:E218A$_{(1:4)}$, and T882S:E218A$_{(4:1)}$ hybrid tetramers (**Fig. 12-14**). The rehybridization of two different PC monomers gives rise to four different combinations of monomers on a single face and 16 unique tetramers, regardless of the relative ratio in which the mutants were mixed. To determine the probability and relative contribution of any unique combination of monomers to the observed catalytic rate, we made four simplifying assumptions, namely that (1) all four positions within the tetramer are equally and independently populated by either monomer type; (2) the positioning of one monomer within the tetramer does not significantly reduce the population of remaining monomers in solution; (3) the activity of a monomer is independent of the activities of the surrounding three monomers within a tetramer; and (4) monomers within a rehybridized mixed tetramer maintain similar activity and apparent K_m or K_a values as their parent homotetramers. For a mixture containing a 1:1 ratio of T882S and E218A monomers, for example (**Fig. 12B**, *all combinations, row 1*), the probability (*p*) that a T882S mutant monomer would fill any of the four positions in the tetramer is given in equation (1), in which *n* and *m* are the relative ratios of T882S and E218A in solution, respectively.

$$p = \frac{n}{n+m} = \frac{1}{1+1} = \frac{1}{2} \qquad (1)$$

Similarly, the probability (q) of an E218A mutant monomer filling any position in the tetramer in a 1:1 mixture of mutants is given in equation (2).

$$q = \frac{m}{n+m} = \frac{1}{1+1} = \frac{1}{2} \qquad (2)$$

Because the numbers of T882S and E218A monomers in solution are very large, these probabilities do not change when a monomer is recombined within one tetramer. Therefore, the probability (P) for forming any one of the 16 unique tetramers is determined by equation (3), in which k is the number of T882S monomers in the configuration (i.e., 0-4) and p and q are the probabilities of T882S or E218A occupying any position in the tetramer, respectively.

$$P = p^k q^{4-k} \qquad (3)$$

In the 1:1 mixture of T882S and E218A monomers, the probability of generating a hybrid tetramer containing a T882S monomer in all four positions (**Fig. 12B**, *combination 1*) is given in equation (4):

$$P = \left(\frac{1}{2}\right)^4 \left(\frac{1}{2}\right)^0 = \left(\frac{1}{2}\right)^4 = 0.0625 \qquad (4)$$

In this same mixture, the probability for an E218A monomer occupying all four positions (**Fig. 12B**, *combination 2*) within a single tetramer is given in equation (5):

$$P = \left(\frac{1}{2}\right)^0 \left(\frac{1}{2}\right)^4 = \left(\frac{1}{2}\right)^4 = 0.0625 \qquad (5)$$

Similar reasoning can be used to determine the probability of distribution for 1:4 and 4:1 mixtures of T882S and E218A mutant monomers. For example, the probability (p) of positioning a T882S monomer in any position of the tetramer in a 1:4 mixture of T882S and E218A is:

$$p = \frac{n}{n+m} = \frac{1}{1+4} = \frac{1}{5} \qquad (6)$$

The probability (q) of positioning the E218A mutant within the tetramer in the same solution is:

$$q = \frac{n}{n+m} = \frac{4}{1+4} = \frac{4}{5} \qquad (7)$$

Combining equations (6) and (7) with equation (3) yields the probability (P) of generating a mixed hybrid tetramer with all T882S monomers (**Fig. 12B**, *combination 1*) in a 1:4 mixture, which is:

$$P = \left(\frac{1}{5}\right)^4 \left(\frac{4}{5}\right)^0 = \left(\frac{1}{5}\right)^4 = 0.0016 \qquad (8)$$

By contrast, the probability of generating a mixed hybrid tetramer with all E218A monomers (**Fig. 12B**, *combination 2*) in a 1:4 mixture is:

$$P = \left(\frac{1}{5}\right)^0 \left(\frac{4}{5}\right)^4 = \left(\frac{4}{5}\right)^4 = 0.41 \qquad (9)$$

To determine the contribution of a particular configuration to the overall observed rate of pyruvate carboxylation, we used the relative positioning of the monomers within the configuration to determine unique intermolecular BC—CT domain interactions that would give rise to catalytic activity. There are four possible catalytically relevant interactions within a single tetramer (BC_1—CT_2, BC_2—CT_1, BC_3—CT_4 and BC_4—CT_3). For example, in configurations 3-6 (**Fig. 12**), each tetramer contains three T882S monomers and one E218A monomer, giving rise to two catalytic interactions between a T882S BC and CT domain (BC_{T882S}—CT_{T882S}), one T882S BC domain interaction with an E218A CT domain interaction (BC_{T882S}—CT_{E218A}), and one E218A BC domain interaction with a T882S CT domain (BC_{E218A}—CT_{T882S}). Based on the relative activities determined for the parent homotetramers, we can assign these interactions with a relative percent activity (i.e., the BC_{T882S}—CT_{T882S} interaction produces 1.6% of wild-type activity, the BC_{T882S}—CT_{E218A} interaction produces 3-5% of wild-type activity, and the BC_{E218A}—CT_{E218A} interaction is inactive). Moreover, because of the finite sample space and the independence of the individual configurations, the probability of any event is the sum of the probability of its elements. In this way, we can combine the probability of distribution with the relative rates of each interaction within the configuration to determine the extent to which the configuration contributes to the overall k_{cat} and determine predicted k_{cat} values for pyruvate carboxylation for the 1:1, 1:4 and 4:1 T882S:E218A hybrid tetramers (**Fig. 12B**). Similar

probability analysis and predicted rates are given for the WT:E218A$_{(1:1)}$ (**Fig. 13**) and the WT:T882S$_{(1:1)}$ (**Fig. 14**) hybrid tetramers.

These methods were also used to predict rates for pyruvate-stimulated release of inorganic phosphate (P_i) catalyzed by the T882S:E218A$_{(1:1)}$ (**Fig. 15**), WT:T882S$_{(1:1)}$ (**Fig. 16**), and WT:E218A$_{(1:1)}$ (**Fig. 17**) hybrid tetramers. Probability distribution was determined as above, but in this case, the relative rate contribution was determined based on either an intramolecular or an intermolecular interaction. Were the mechanism intramolecular in nature, the rate of P_i release from the active T882S BC domains in the presence of saturating concentrations of pyruvate would be solely controlled by the T882S CT domains on the same monomers. For example, in configurations 3-6, three of the four PC monomers in the hybrid tetramer will exhibit activity consistent with the BC domain activity of the T882S holoenzyme (1.2% of wild-type activity), regardless of the identity of, or interactions with, other monomers in the tetramer. The single E218A BC domain in this configuration would be controlled by its own CT domain. Alternatively, if we were to assume an intermolecular mechanism, pyruvate binding in the CT domain of an opposing polypeptide chain would stimulate the BC domain reaction, and we would see that the calculated rate of P_i release for the same configuration is dependent upon two T882S CT domain interactions (BC_{T882S}—CT_{T882S}, 1.2% of wild-type activity) and one E218A CT domain interaction (BC_{T882S}—CT_{E218A}, 3-5% of wild-type activity) with any of the three catalytically active T882S BC domains. Again, since the events occur independently, the probability and overall calculated k_{cat} is the sum of all events.

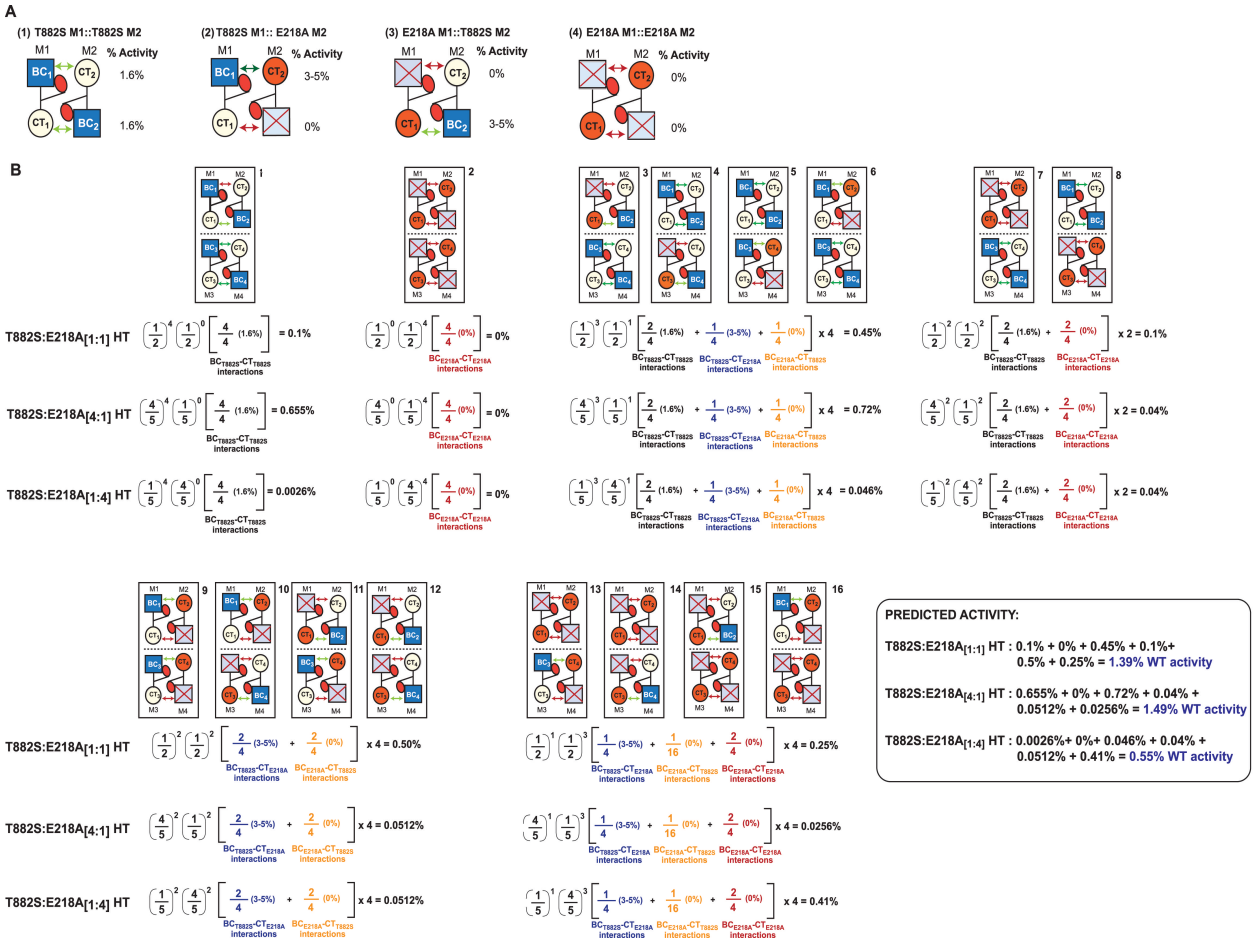

FIGURE 12. Probability analysis for rehybridization of T882S and E218A mutants in a 1:1, 1:4, or 4:1 ratio, and predicted pyruvate carboxylation activity for each possible tetramer combination. (A) Rehybridization of the T882S and E218A mutant monomers of PC yields four unique combinations of monomers within a single face of the tetramer. Faces in which both monomers are T882S or E218A are predicted to exhibit 1.6% and 0% pyruvate carboxylation activity relative to the wild-type, respectively. (B) Statistically random rehybridization of T882S and E218A monomers produces 16 possible tetramers with unique compositions. Probability of each configuration is denoted in rounded brackets, and overall catalytic contribution of each configuration is denoted in squared brackets.

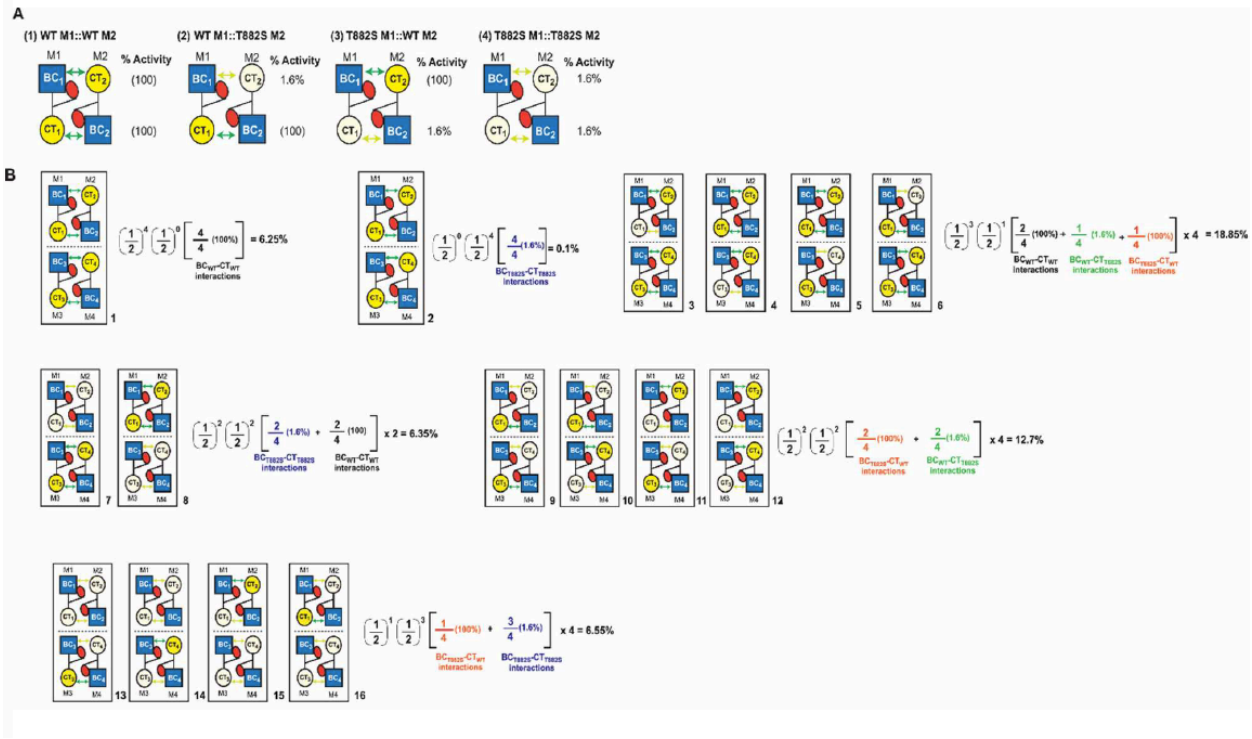

FIGURE 13. Probability analysis for rehybridization and predicted pyruvate carboxylation activity of wild-type and T882S mutants in a 1:1 ratio. (A) Rehybridization of the wild-type and T882S monomers of PC. Faces in which both monomers are T882S are predicted to exhibit 1.6% pyruvate carboxylation activity relative to the wild-type. (B) 16 possible tetramer compositions upon statistically random rehybridization of wild-type and T882S monomers.

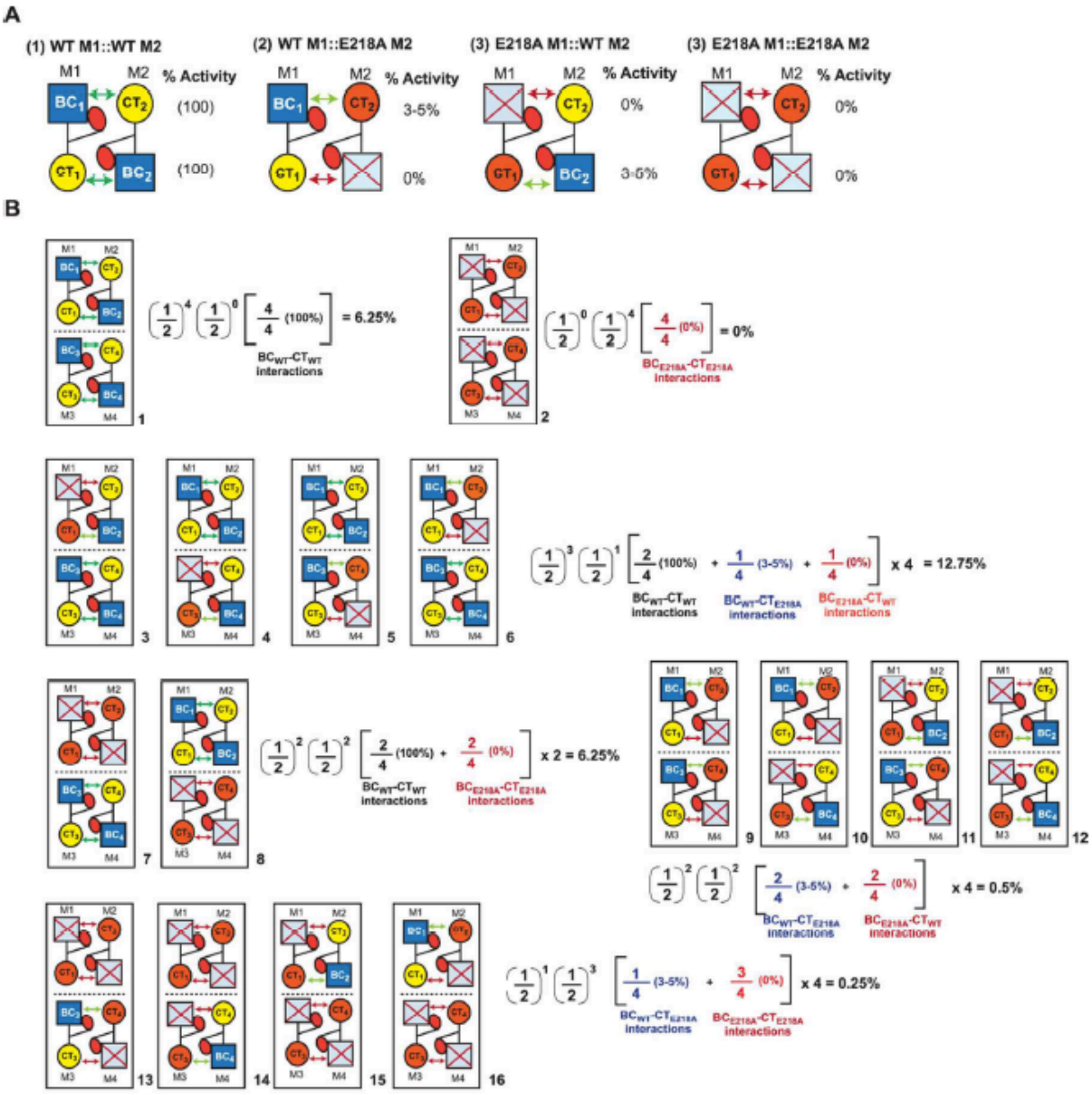

FIGURE 14. Probability analysis for rehybridization and predicted pyruvate carboxylation activity of wild-type and E218A mutants in a 1:1 ratio. (A) Rehybridization of the wild-type and E218A monomers of PC. Faces in which both monomers are T882S are predicted to exhibit 0% pyruvate carboxylation activity relative to the wild-type. (B) 16 possible tetramer compositions upon statistically random rehybridization of wild-type and E218A monomers.

FIGURE 15. Predicted activity for intra- or intermolecularly controlled pyruvate-stimulated P_i release by T882S:E218A$_{(1:1)}$ hybrid tetramers. For the intramolecular mechanism, the rate of P_i release would be controlled by the CT domain on the same monomer; in this hybrid tetramer, the rate of P_i release would be due solely to the T882S monomers in the tetramer, given that the BC domain of E218A is inactive. Alternatively, for the intermolecular mechanism, the rate of P_i release would be influenced by the CT domain on the opposing polypeptide chain; in this case, the CT domain of E218A would affect the activity when paired with a BC domain of a T882S monomer.

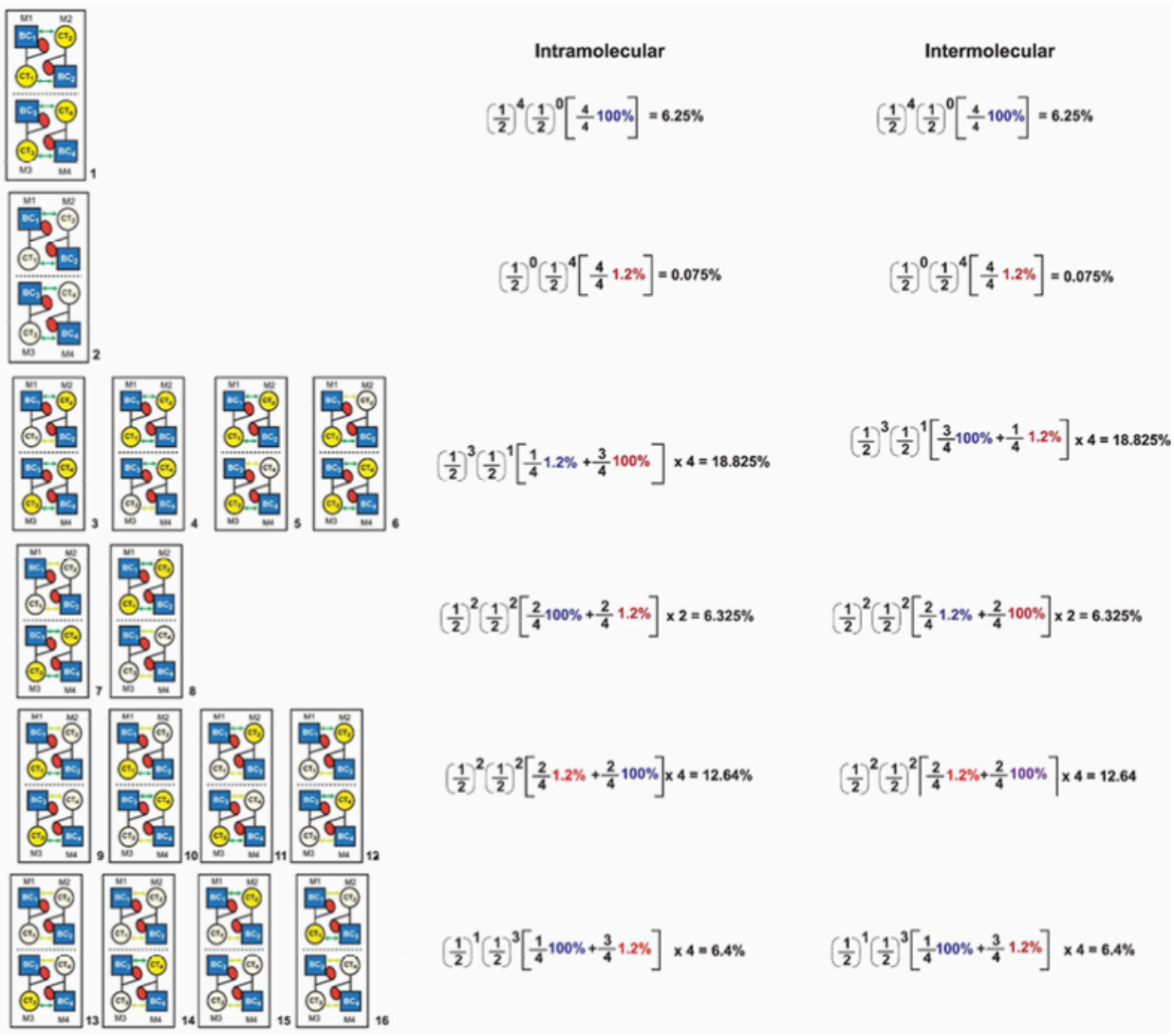

FIGURE 16. Predicted activity for intra- or intermolecularly controlled pyruvate-stimulated P_i release by WT:T882S$_{(1:1)}$ hybrid tetramers. For the intermolecular mechanism, the CT domain of the wild-type would have an effect on activity and contribute to the catalytic rate when paired with a T882S BC domain.

FIGURE 17. Predicted activity for intra- or intermolecularly controlled pyruvate-stimulated P_i release by WT:E218A$_{(1:1)}$ hybrid tetramers. For the intermolecular mechanism, the CT domain of the E218A monomer would have an effect on activity and contribute to the catalytic rate when paired with a wild-type BC domain.

Pyruvate Carboxylation Activity. V_{max} and $(V/K)_{pyruvate}$ values were determined by fitting initial velocity plots to the Michaelis-Menten equation (equation 10) using nonlinear regression analysis. In this equation, V_{max} represents the maximum achievable initial rate, v_i represents the initial rate at a given concentration of pyruvate, and K_m is the Michaelis-constant. Error bars are the standard deviation from the mean of three individual determinations. All fits were performed using GraphPad Prism (v. 6).

$$v_i = \frac{V_{max}[pyruvate]}{K_m + [pyruvate]} \qquad (10)$$

Determination of Initial Rates of P_i Release from the BC Domain. Initial velocity data were fitted to equation (11), in which k_0 (sec^{-1}) represents the rate of P_i release occurring in the absence of pyruvate and K_a is the apparent K_m of pyruvate for P_i release. Error bars are the standard deviation from the mean of three individual determinations.

$$v_i = k_0 + \frac{V_{max}[pyruvate]}{K_a + [pyruvate]} \qquad (11)$$

RESULTS

Comparison to Previously Reported Data for Pyruvate Carboxylation.

In previous work, the k_{cat} and $K_{m\ pyruvate}$ were determined for wild-type *Re*PC and reported to be 7.1 ± 0.9 min^{-1} and 0.47 ± 0.04 mM, respectively (11). These results were obtained in the presence of the substrate HCO_3^- with a concentration of 15 mM, which is sub-saturating, as the $K_{m\ HCO3}$ is 10 mM (**Table 1**). When this concentration was used, an increase in $K_{m\ pyruvate}$ to 0.54 ± 0.08 mM was observed, which is a 2.5-fold increase from the $K_{m\ pyruvate}$ obtained at 40 mM HCO_3^- (0.22 ± 0.3 mM). Also under these previous conditions, a hyperbolic 1:1 coupling ratio between the rates of oxaloacetate production in the CT domain and inorganic phosphate release from the BC domain (OAA/P_i) was observed. The k_{cat} OAA/k_{cat} P_i release ratio produced in this study demonstrated a linear dependence on pyruvate concentration rather than hyperbolic, which was observed at 15 mM HCO_3^-. The implications of this reduced substrate concentration will be discussed, and for the purposes of the experiments performed in this study, we have modified the experimental design to include saturating (40 mM) concentrations of HCO_3^-.

Pyruvate Carboxylation Activity and Oxaloacetate Formation.

The k_{cat} (sec^{-1}) and $k_{cat}/K_{m\ pyruvate}$ (sec^{-1} mM^{-1}) for pyruvate carboxylation were measured by determining the initial rates of oxaloacetate formation for the wild-type, T882S mutant, and hybrid tetramer forms of *Re*PC (**Fig. 18, 19**). Oxaloacetate formation was measured at varying concentrations of pyruvate (0.25 – 40 mM) and saturating concentrations of the BC domain substrates, MgATP and HCO_3^-, and the activator, acetyl-CoA, through conversion to malate via

malate dehydrogenase. All forms of the enzyme and the hybrid tetramers exhibited normal Michaelis-Menten type responses across increasing concentrations of the substrate pyruvate.

The Glu218 residue is one of three comprising the catalytic triad of the MgATP and HCO_3^- binding pockets in the BC domain, along with Lys245 and Glu305, and is required in order for MgATP-cleavage to occur (**Fig. 10**) (6). Mutation of Glu218 to Ala (E218A), which was characterized previously, completely abolished BC domain activity, preventing use of the mutant as a homotetramer for measurement of pyruvate carboxylation. However, the mutant retained wild-type affinity for pyruvate binding in its CT domain and 3-5% of wild-type activity, and thus was recognized as ideal for studying the effects of individual domains on overall coordination of catalysis.

Also demonstrated previously was the critical nature of the strictly conserved Thr882 residue (**Fig. 8**), which is located in the pyruvate binding site of the CT domain and required for proton shuttling between the biotin enolate and bound pyruvate to form oxaloacetate (7, 15). By mutating Thr882 conservatively to Ser (T882S), the hydroxyl functional group required for proton shuttling was conserved in the active site, though in an altered position relative to the biotin enolate and pyruvate, causing significant impairment of the mutant's catalytic activity (**Fig. 18**). Relative to the wild-type, the T882S mutation, which was characterized in the present study (**Table 1**), exhibited a 62-fold decrease in k_{cat} (0.166 ± 0.005 s^{-1}) and a 360-fold decrease in k_{cat}/K_m (0.13 ± 0.02 s^{-1} mM^{-1}). The T882S mutant also exhibited a 6-fold increase in $K_{m\ pyruvate}$ (1.3 ± 0.2 mM) for the pyruvate carboxylation reaction relative to the wild-type (0.22 ± 0.03 mM) mM). This discrepancy in the K_m made the T882S mutant also an ideal candidate for use in

generating hybrid tetramers. Hybrid tetramers were first generated using the wild-type and mutant forms of PC, mixed in equal ratios (WT:T882S$_{(1:1)}$ and WT:E218A$_{(1:1)}$). The WT:T882S$_{(1:1)}$ hybrid tetramer mixture was initially generated as a control to compare against the wild-type form (10.3 ± 0.2 s^{-1}) and the T882S mutant homotetramer, exhibiting a 3-fold decrease relative to the wild-type and 20-fold increase in activity relative to the T882S homotetramer (3.26 ± 0.06 s^{-1}), respectively (**Table 1**). This pyruvate carboxylation activity was lower than predicted, which we attributed either to insufficient rehybridization of the monomers or failure of the tetramer to completely couple MgATP-cleavage with oxaloacetate formation. Were this rate reduction due to failure of the monomers to rehybridize in solution once mixed, our entire methodology would be flawed, as we would not be able to reliably attribute any reduction in the rate to signaling effects observed between monomers of different activities and substrate affinities. Alternatively, if the hybrid tetramer was truly failing to couple the BC and CT domain reactions, then our methodology would be sound and the reduction in pyruvate carboxylation activity could be reconciled by the T882S CT domain's drastically impaired ability to associate with pyruvate in a significant enough manner to prompt BCCP domain egress from the BC domain active site, or to remain associated with pyruvate long enough for the opposing polypeptide chain's BCCP domain to complete translocation.

The WT:E218A$_{(1:1)}$ hybrid tetramer was then generated and its pyruvate carboxylation activity at 40 mM pyruvate was measured. This hybrid tetramer again exhibited a 3-fold reduction in rate (3.23 ± 0.01 s^{-1}) relative to the wild-type; however, when predicted activity was determined for this mixture of monomers based on the probability of monomer arrangements within the tetramer and the relative contribution of each monomer's activity to the overall catalytic rate, the

calculated k_{cat} was 3.32 ± 0.02 s^{-1}, which is comparable to the reduced observed rate. Based on this calculation, we considered the methodology of rehybridization sound and attributed the reduced rates to coupling efficiency rather than to insufficient rehybridization of monomers. Furthermore, we will present results from analysis of additional combinations of hybrid tetramers which confirm that the reduced catalytic rate relative to expected values is due to a reduction in coupling efficiency of MgATP-cleavage and oxaloacetate formation.

		k_{cat} observed (s^{-1})	% WT activity	k_{cat} calculated (s^{-1})	% WT activity	$K_{m,\ pyruvate}$ (mM)	k_{cat}/K_m (s^{-1} mM^{-1})
WT	15 mM HCO_3^-	1.25 ± 0.04	—	—	—	0.54 ± 0.08	2.3 ± 0.4
	40 mM HCO_3^-	10.3 ± 0.2	(100)	—	(100)	0.22 ± 0.03	47 ± 6
T882S		0.166 ± 0.005	1.6	—	—	1.3 ± 0.2	0.13 ± 0.02
E218A		NA	0	—	0	—	—
WT:T882S$_{(1:1)}$		3.26 ± 0.06	31	5.2 ± 0.1	51	0.33 ± 0.03	9.9 ± 0.9
WT:E218A$_{(1:1)}$		3.23 ± 0.01	31	3.32 ± 0.02	32	ND	ND
T882S:E218A$_{(1:1)}$		0.075 ± 0.002	0.7	0.143 ± 0.003	1.4	0.20 ± 0.03	0.38 ± 0.06
T882S:E218A$_{(4:1)}$		0.165 ± 0.004	1.6	0.152 ± 0.003	1.5	0.8 ± 0.1	0.21 ± 0.03
T882S:E218A$_{(1:4)}$		0.121 ± 0.006	1.2	0.058 ± 0.001	0.6	1.6 ± 0.3	0.081 ± 0.001

TABLE 1. Initial rates of pyruvate carboxylation activity for the wild-type at subsaturating (15 mM) and saturating (40 mM) concentrations of HCO_3^-, as well as the T882S homotetramer and the WT:T882S$_{(1:1)}$, WT:E218A$_{(1:1)}$, and T882:E218A (mixed in ratios of 1:1, 4:1, and 1:4) hybrid tetramers. For each of the hybrid tetramer mixtures, the k_{cat} was calculated based on the probability analysis of possible monomer arrangements within each tetramer, as well as the relative contribution to the rate of pyruvate carboxylation of each type of monomer.

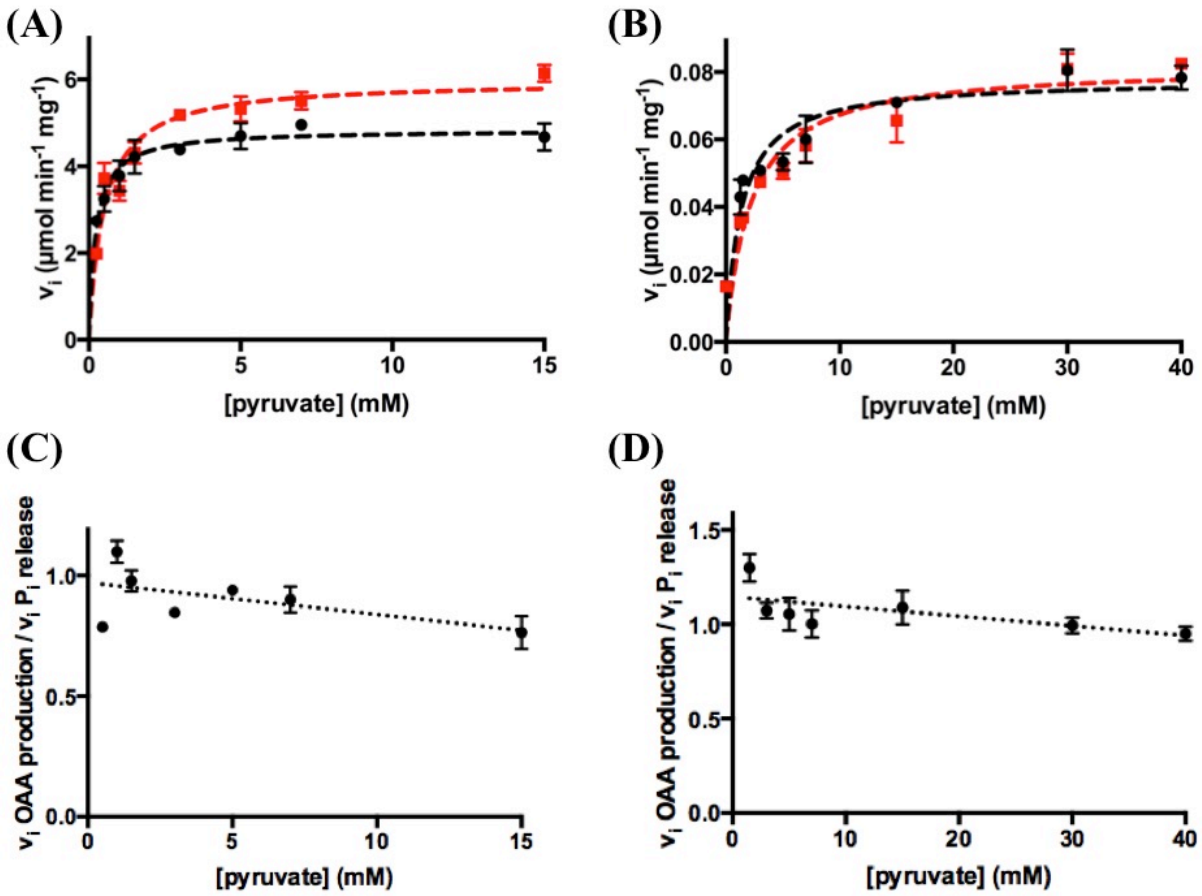

FIGURE 18. Initial rates of pyruvate carboxylation (●) and pyruvate-stimulated P_i release (■) for the wild-type (*A*) and T882S homotetramer (*B*) as a function of increasing pyruvate concentrations. Coupling ratios for the initial rates of oxaloacetate formation and P_i release for the wild-type (*C*) and T882S (*D*) half-reactions are also shown as a function of pyruvate concentration.

We next generated hybrid tetramers consisting of the T882S and E218A mutant forms of PC by mixing the mutants in a 1:1 ratio (**Fig. 19**). The T882S:E218A$_{(1:1)}$ hybrid tetramer exhibited a k_{cat} of 0.075 ± 0.002 s^{-1}, which was about half of the activity predicted (0.143 ± 0.003 s^{-1}), and a $K_{m,pyruvate}$ (0.20 ± 0.03 mM) that was 6.5-fold lower than that of the T882S homotetramer (**Table 1**). Given that the significant reduction in rate relative to predicted values was also observed in the WT:T882S$_{(1:1)}$ hybrid tetramer, we next considered the possibility that the T882S mutant itself could be hindering tetramerization of the enzyme, and generated hybrid tetramers of the T882S and E218A mutants mixed in 4:1 and 1:4 ratios to measure the rates of pyruvate carboxylation in excess of either mutant (**Table 1**). Observed activity of the T882S:E218A$_{(4:1)}$ mixture (0.165 ± 0.004 s^{-1}) matched the predicted rate (0.152 ± 0.003 s^{-1}), and the apparent $K_{m\ pyruvate}$ (0.8 ± 0.1 mM), which was 4-fold higher than that of the wild-type, can be attributed to the increased prevalence of T882S monomers within the rehybridized tetramers. The T882S:E218A$_{(1:4)}$ hybrid tetramers exhibited twice the activity of the predicted rate of pyruvate carboxylation (0.121 ± 0.006 s^{-1} observed versus 0.058 ± 0.001 s^{-1} predicted) with an apparent $K_{m\ pyruvate}$ nearly equivalent to that of the T882S homotetramer (1.6 ± 0.3 mM). Based on these observed values relative to predicted rates, we believe that discrepancies are due to the impaired ability of the T882S monomers to retain control of coupling between BC and CT domain reactions.

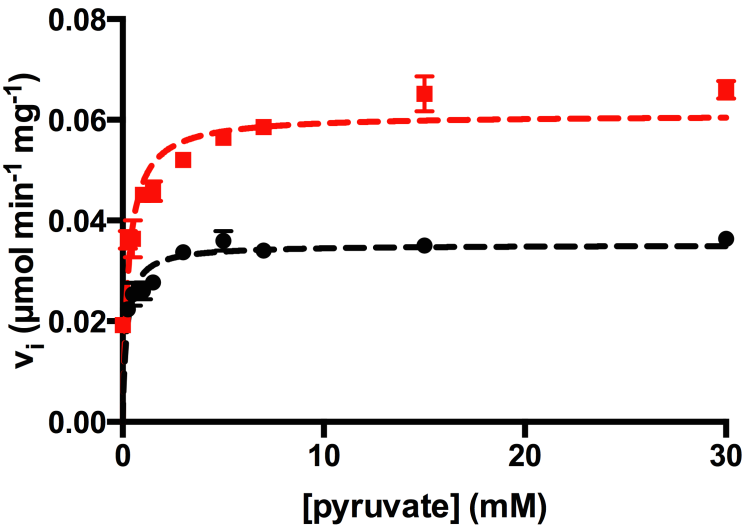

FIGURE 19. Initial rates of pyruvate carboxylation (●) and pyruvate-stimulated P_i release (■) for the T882S:E218A$_{(1:1)}$ hybrid tetramer form of *Re*PC as a function of increasing pyruvate concentration.

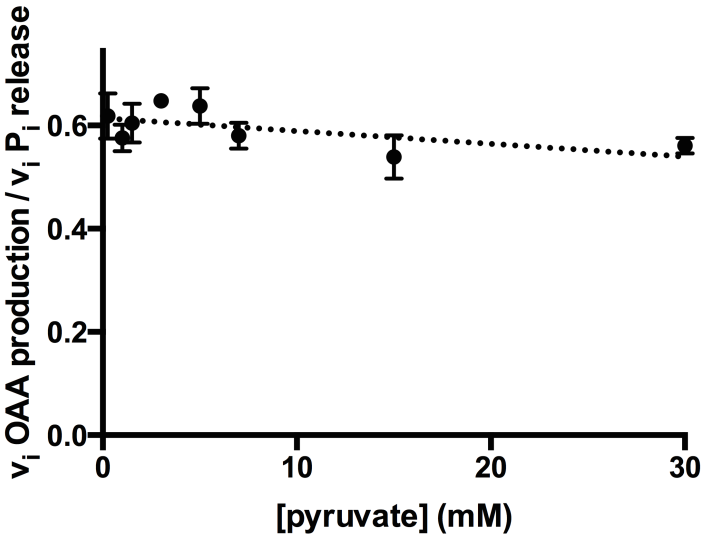

FIGURE 20. Coupling ratios for the initial rates of oxaloacetate formation and P_i release for the T882S:E218A$_{(1:1)}$ hybrid tetramer form of PC.

MgATP-Cleavage and Inorganic Phosphate Release in the Presence and Absence of Pyruvate.

The initial rates of MgATP-cleavage and P_i release, occurring within the BC domain, were measured in the presence (**Table 2**) and absence (**Table 3**) of pyruvate to determine the k_{cat} (sec^{-1}) and $k_{cat}/K_{m\ pyruvate}$ for the wild-type, mutant homotetramers, and mixed hybrid tetramers. While P_i release is largely stimulated by pyruvate occupancy in the CT domain, a level of pyruvate-independent P_i release also occurs due to small, random motions of the BCCP domain and vibrations inherent in the enzyme structure which allow the biotin cofactor to transiently exit the BC domain binding pocket, thus releasing MgADP and P_i that is not productively utilized for oxaloacetate formation. The T882S homotetramer exhibited a 17-fold decrease in rate of P_i release ($0.043 \pm 0.006\ s^{-1}$) relative to the wild-type ($0.73 \pm 0.09\ s^{-1}$), and the E218A homotetramer yielded no measurable activity due to its defunct BC domain.

The rate of P_i release in the WT:E218A$_{(1:1)}$ hybrid tetramer mixture ($0.249 \pm 0.009\ s^{-1}$) was 34% lower than that observed for the wild-type; while this difference is significant, we had expected a 50% reduction in activity due to half of the BC domains in this ratio being inactive. The WT:T882S$_{(1:1)}$ hybrid tetramer was 50% as active as the wild-type ($0.33 \pm 0.07\ s^{-1}$), and higher in activity than the T882S homotetramer, as we anticipated. The T882S:E218A$_{(1:1)}$ hybrid tetramer, in a similar pattern as the WT:E218A$_{(1:1)}$, catalyzed P_i release at a 3-fold lower rate than the T882S homotetramer.

Initial rates of P_i release were also measured in the presence of varying concentrations of pyruvate (0.25 – 40 mM) and saturating concentrations of all other substrates and activators. In this case, the apparent $K_{a\ pyruvate}$ was taken to represent the ability of the CT domain to induce

BCCP domain translocation and not necessarily the ability to carboxylate pyruvate. In the presence of pyruvate, the T882S homotetramer yielded a 3.4-fold higher rate of P_i release (0.146 ± 0.005 s^{-1}) than in its absence, and the apparent K_a was approximately 4-fold greater than the $K_{m\ pyruvate}$ observed for pyruvate carboxylation. The apparent K_a for the T882S homotetramer (5.4 ± 0.6 mM) was also 10-fold higher than that of the wild-type (0.56 ± 0.07 mM). Taken together, the larger K_a and reduction in k_{cat} yield a 780-fold reduction in k_{cat}/K_m for the T882S homotetramer relative to the wild-type (0.027 ± 0.003 s^{-1} mM^{-1} versus 21 ± 3 s^{-1} mM^{-1}), which is suggestive of the impaired ability of T882S *Re*PC to induce BCCP translocation.

	k_{cat} observed (s^{-1})	% WT activity
WT	0.73 ± 0.09	(100)
T882S	0.043 ± 0.006	6
E218A	NA	0
WT:E218A$_{(1:1)}$	0.249 ± 0.009	34
WT:T882S$_{(1:1)}$	0.33 ± 0.07	45
T882S:E218A$_{(1:1)}$	0.0134 ± 0.002	2

TABLE 2. Initial rate of inorganic phosphate release activity in the absence of pyruvate for the wild-type, T882S and E218A mutant homotetramers, and hybrid tetramer forms of PC.

	k_{cat} observed (s^{-1})	% WT activity	$K_{a,\ pyruvate}$ (mM)	k_{cat}/K_a (s^{-1} mM^{-1})
WT	12.1 ± 0.4	(100)	0.56 ± 0.07	21 ± 3
T882S	0.146 ± 0.005	1.2	5.4 ± 0.6	0.027 ± 0.003
E218A	NA	0	—	—
WT:T882S$_{(1:1)}$	6.6 ± 0.1	55	0.91 ± 0.07	7.3 ± 0.6
WT:E218A$_{(1:1)}$	3.78 ± 0.07	31	ND	ND
T882S:E218A$_{(1:1)}$	0.118 ± 0.003	0.9	0.37 ± 0.05	0.32 ± 0.04

TABLE 3. Observed initial rates of inorganic phosphate release activity in the presence of pyruvate for the wild-type; the T882S homotetramer; and the WT:T882S$_{(1:1)}$, WT:E218A$_{(1:1)}$, and T882S:E218A$_{(1:1)}$ hybrid tetramers.

The question still remained as to which CT domain within a face of the enzyme controls translocation of the BCCP domain, which led us to determine the rates of P_i release for hybrid tetramers combining the wild-type with the mutant forms, as well as combining both mutants together. Calculation of predicted rates that would correspond to intramolecular or intermolecular mechanisms (**Table 4**), and comparison of the observed rates of P_i release, allowed us to determine which of the two mechanisms of subunit communication is most likely occurring during the catalytic cycle of PC.

The ability of the WT:E218A$_{(1:1)}$ hybrid tetramer to cleave MgATP was measured at 40 mM pyruvate and yielded an initial rate of 3.78 ± 0.07 s^{-1}, which was approximately 15-fold higher than the rate in the absence of pyruvate. Upon examination of the arrangement of monomers within the WT:E218A$_{(1:1)}$ tetramer, it is possible to calculate the rate of P_i release relative to the wild-type for an intra- versus intermolecular mechanism. Due to the defunct BC domain of the E218A mutation, all observed BC domain activity must be due to the BC domains of the wild-type subunits. Were the mechanism intramolecular in nature, binding of pyruvate to the CT domain of one polypeptide chain would induce movement of the BCCP domain on the same monomer, so all of the CT domains in the WT:E218A$_{(1:1)}$ hybrid tetramer would induce BCCP domain translocation only on the wild-type subunits; this would result in a rate of P_i release approximately half that of the wild-type homotetramer. Alternatively, were the mechanism an intermolecular one, pyruvate binding in the CT domain of one polypeptide chain would induce BCCP translocation of the opposing polypeptide chain, "pulling" the BCCP domain over to itself. In this case, pyruvate binding in either the wild-type or E218A CT domain could elicit BCCP translocation from an opposing chain, depending on arrangement of the monomers in the

tetramer (**Fig. 21**). Given that the E218A CT domain retains 3-5% of wild-type pyruvate carboxylation activity, this mechanism would result in P_i release at a rate of 26% of the wild-type activity. The observed rate of P_i release was 31% of that of the wild-type, which was consistent with the signaling mechanism being intermolecular in nature.

The T882S:E218A$_{(1:1)}$ hybrid tetramer was also examined to further elucidate the signaling mechanism governing BCCP translocation and P_i release from the BC domain. Just as with the WT:E218A$_{(1:1)}$ hybrid tetramer, it is possible to predict the rate of P_i release for the T882S:E218A$_{(1:1)}$ hybrid tetramer under an intra- or intermolecular signaling mechanism. For an intramolecular control mechanism, the T882S CT domain would govern translocation of its own BCCP domain; in that case, we would expect apparent $K_{a\ pyruvate}$ values similar to that of the T882S homotetramer and an initial rate of P_i release about 0.6% of that of the wild-type. For an intermolecular mechanism, the E218A CT domain would be responsible for translocation of the opposing T882S BCCP domain; this would yield an apparent $K_{a\ pyruvate}$ significantly lower than that of the T882S homotetramer and a rate of 0.9% wild-type activity. The apparent $K_{a\ pyruvate}$ for the T882S:E218A$_{(1:1)}$ hybrid tetramer (0.20 ± 0.03 mM) was 1.5-fold lower even than that observed for the wild-type, and 15-fold lower than that of the T882S homotetramer. These results are consistent with an intermolecular mechanism of subunit communication, in which pyruvate binding to the CT domain of the E218A mutant, which has wild-type affinity for pyruvate, is in control of inducing translocation of the BCCP domain on the T882S mutant.

	k_{cat} calculated, intermolecular (s^{-1})	% WT activity	k_{cat} calculated, intramolecular (s^{-1})	% WT activity
WT	—	(100)	—	(100)
T882S	—	—	—	—
E218A	—	—	—	—
WT:T882S$_{(1:1)}$	6.1 ± 0.2	50.5	6.1 ± 0.2	50.5
WT:E218A$_{(1:1)}$	3.1 ± 0.1	26	6.0 ± 0.2	50
T882S:E218A$_{(1:1)}$	0.133 ± 0.004	1.1	0.073 ± 0.002	0.6

TABLE 4. Calculated initial rates of inorganic phosphate release based on an intermolecular or intramolecular mechanism of BCCP domain control. Values were compared to initial rates obtained in Table 3 to determine whether data more closely matched one mechanism of control than the other.

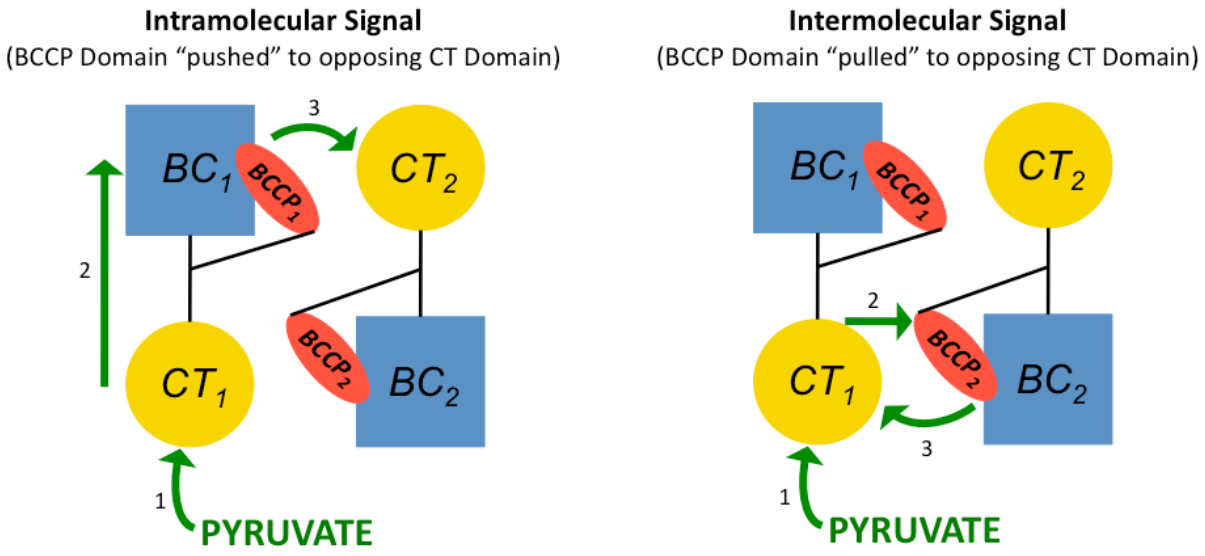

FIGURE 21. Schematic of intra- and intermolecular mechanisms of signaling in RePC. *Left*: were the signal intramolecular in nature, pyruvate binding in one CT domain (arrow 1) signals carboxylation of the covalently attached biotin on its own BCCP domain (arrow 2) and translocation to the opposing polypeptide chain (arrow 3). Pyruvate binding causes the BCCP domain to be "pushed" to the opposing CT domain for catalysis. *Right*: for an intermolecular signaling mechanism, pyruvate binding in one CT domain (arrow 1) signals to the BCCP domain on the opposing polypeptide chain (arrow 2) and "pulls" the BCCP domain, containing the carboxybiotin intermediate, over to itself.

Coupling of BC and CT Domain Reactions.

The extent of coupling between oxaloacetate formation following pyruvate carboxylation in the CT domain and inorganic phosphate release as a result of MgATP-cleavage in the BC domain was determined by measuring the formation of each under varying concentrations of pyruvate (0.25 – 40 mM) and otherwise identical conditions for the wild-type, T882S, T882S:$WT_{(1:1)}$, and T882S:$E218A_{(1:1)}$ tetramers (**Table 5**). A ratio of the k_{cat} of oxaloacetate production to the k_{cat} of inorganic phosphate release approaching one is indicative of complete coupling between the two domain half-reactions, meaning that MgATP-cleavage is efficient and productive, resulting in oxaloacetate formation. As the ratio decreases, coupling of the two reactions becomes incomplete, resulting in nonproductive MgATP-cleavage. The ratio also should not exceed one, as cleavage of at least one MgATP molecule is necessary to form one oxaloacetate molecule. At saturating concentrations of pyruvate, nearly complete coupling was exhibited by the wild-type, the T882S homotetramer, and the WT:$E218A_{(1:1)}$ hybrid tetramer (**Fig. 18**), whereas the ratios for the WT:$T882S_{(1:1)}$ and T882S:$E218A_{(1:1)}$ hybrid tetramers were approximately 0.5 – 0.6, indicating significant loss of coupling between the BC and CT domains upon introduction of the T882S mutant (**Fig. 20**).

The ratio of rates of oxaloacetate formation to P_i release demonstrated linear dependence on pyruvate concentration for the wild-type, T882S homotetramer, and all mixed hybrid tetramers, which was surprising, given that a hyperbolic dependence was observed in previous work. However, we attribute this again to the subsaturating concentrations of HCO_3^- used in those studies, especially because the concentration of HCO_3^- has been shown here to have a significant impact on the $K_{m\ pyruvate}$ for pyruvate carboxylation activity of PC.

In all, these results serve to suggest that BCCP domain translocation is governed by an intermolecular signaling mechanism, whereby pyruvate binding in the CT domain of one monomer controls BCCP translocation on the opposing polypeptide chain. Additionally, mixed hybrid tetramers containing the T882S mutant form of *Re*PC lost BC and CT domain coupling, leading to nonproductive MgATP-cleavage at a rate of nearly two MgATP cleaved per oxaloacetate formed.

	k_{cat} OAA formation / k_{cat} P_i release	k_{cat}/K_m OAA formation / k_{cat}/K_a P_i release
WT	0.85 ± 0.03	2.2 ± 0.4
T882S	1.1 ± 0.9	4.8 ± 0.9
WT:T882S$_{(1:1)}$	0.49 ± 0.01	1.4 ± 0.2
WT:E218A$_{(1:1)}$	0.85 ± 0.02	ND
T882S:E218A$_{(1:1)}$	0.64 ± 0.02	1.2 ± 0.2

TABLE 5. Coupling ratio of initial rates of oxaloacetate production to inorganic P_i release for *Re*PC wild-type, the T882S mutant form, and the hybrid tetramer combinations shown. K_m represents the $K_{m\ pyruvate}$ for pyruvate carboxylation activity, and K_a represents the apparent $K_{a\ pyruvate}$ for P_i release activity.

DISCUSSION

Previous studies have demonstrated that pyruvate binding in the CT domain has a significant stimulatory effect on translocation of the BCCP domain, specifically in the presence of acetyl-CoA, thus promoting movement away from the BC domain and release of P_i.(6, 11, 13, 27) It has also been shown that the presence of increasing concentrations of pyruvate present in the CT domain decreases nonproductive cleavage of MgATP in the BC domain; that is, the proportion of MgATP cleavages occurring that result in formation of oxaloacetate increases (28). While pyruvate binding does not affect the global conformation of the enzyme, it does prompt structural alterations within the CT domain and near its active site, such that the required binding pocket for the carboxybiotin intermediate is formed (5). Together, these findings seem to indicate that the ability of pyruvate to coordinate catalysis is dependent on successfully inducing translocation of the BCCP domain, as well as remaining bound in the CT domain for long enough to interact with the carboxybiotin intermediate.

Our studies have sought to answer the question of whether pyruvate binding at the CT domain of one polypeptide chain within a face facilitates translocation of the BCCP domain through an intra- or intermolecular communication mechanism, and generation of mixed hybrid tetramers has allowed us to distinguish between the two (**Fig. 21**). Only the T882S:E218A$_{(1:1)}$ hybrid tetramer allows observation of significant catalytic activity by determining the k_{cat} and apparent $K_{a\ pyruvate}$ for P_i release. In this equal mixture of mutant monomers, the activity of which was calculated through probability analysis of the possible monomer positions within the tetramer, only a combination of T882S and E218A monomers within a single face would produce catalytic

activity. In this case, an intramolecular communication mechanism would be under the control of the T882S CT domain, which has a dramatically reduced binding affinity for pyruvate (manifested as an apparent $K_{a\ pyruvate}$ of P_i release that is 10-fold higher than that of the *Re*PC wild-type). On the other hand, an intermolecular mechanism would be under the control of the E218A CT domain, which retains wild-type affinity for pyruvate, as demonstrated by its apparent $K_{a\ pyruvate}$ of P_i release that is approximately half of that of the wild-type.

Initially, we anticipated that PC would function via an intramolecular mechanism, whereby pyruvate binding at one CT domain would facilitate translocation of the BCCP domain on the same polypeptide chain, serving to "push" that BCCP domain to the opposing monomer to carry out catalysis. This possibility seemed to be the more intuitive, in that pyruvate binding would be able to induce conformational shifts within the enzyme through physically connected residue networks between the CT domain, the allosteric domain, and the swinging arm of the BCCP domain. Additionally, this intramolecular mechanism of communication would have accounted for PC's 50% commitment to catalysis once bound to pyruvate, since the CT domain responsible for inducing movement of the BCCP domain (i.e., the CT domain of the T882S monomer, in the T882S:E218A$_{(1:1)}$ hybrid tetramer) would not be the same as the CT domain that is the site of oxaloacetate formation (i.e., the CT domain of the E218A monomer). However, our anticipation that this mechanism would be intramolecular was based largely on the assumption that a discrete, functional residue network between the two active sites not only exists, but is directly responsible for their communication, despite the fact that such a network has yet to be identified experimentally. Current views of allostery do not require direct residue interactions or subsequent conformational changes in order to coordinate catalysis, instead focusing on

thermodynamic characteristics of multifunctional enzymes as the most likely source of communication in allosteric effects. Given that, it becomes possible to conceive of an intermolecular mechanism occurring in PC, whereby communication for catalysis is propagated in the absence of significant conformational shifts through physical residue networks.

Based on the steady-state kinetics analyzed in this study, we have determined that pyruvate binding in one CT domain induces BCCP translocation on the opposing polypeptide chain, consistent with an intermolecular mechanism of communication. An intermolecular mechanism would also explain the incomplete coupling observed between the BC and CT domain half-reactions in the T882S:E218A$_{(1:1)}$ hybrid tetramer, given that both the CT domains of the T882S and E218A monomers, with different affinities for pyruvate, are controlling catalysis on each polypeptide chain. This also gives rise to the possibility of a mechanism involving half-sites reactivity, in which only one BC—CT domain pair on a single face is active at a time, or oscillating catalysis, in which alternating faces are active at a single time.

These experiments do not differentiate between the effects seen within a face as opposed to effects caused by interactions between faces, so we cannot say for sure based on these findings whether the incomplete coupling observed in the hybrid tetramers containing T882S monomers was due to pyruvate binding within the same face or in a CT domain on the opposite face. Further study of additional molecular interactions within the tetrameric structure is needed to elucidate the nature of the mechanism by which PC controls BCCP translocation and the coordination of catalysis between the two spatially distinct active sites within a face.

Through generation of these functional hybrid tetramers using the T882S, with low CT domain activity relative to the wild-type, and E218A, with a defunct BC domain, mutant forms of PC, we have begun to address the method by which spatially separate domains within the tetramer sense pyruvate occupancy in the CT domain. The T882S:E218A$_{(1:1)}$ hybrid tetramer exhibited a near wild-type apparent $K_{a\ pyruvate}$ for P_i release from the BC domain which was almost 10-fold lower than that of the T882S homotetramer. Also, the hybrid tetramer exhibited a loss of coupling between the initial rates of oxaloacetate formation and MgATP-cleavage, with the ratio of the two domain reactions remaining constant at 0.6 regardless of pyruvate concentration. These results collectively indicate a signaling mechanism that is intermolecular in nature, whereby pyruvate binding to one CT domain within a face of the PC tetramer signals BCCP domain translocation on the opposing polypeptide chain, "pulling" the carboxylated biotin cofactor over to itself. Given the complexity of this interaction and the minimal amino acid residue interactions that occur between monomers within a single face, these findings are suggestive of some type of thermodynamic stability as the driving force responsible for allosteric regulation and intersubunit communication in the PC tetramer.

CHAPTER 2 – THERMODYNAMIC LINKAGE ANALYSIS OF SUBSTRATE BINDING AT SPATIALLY DISTINCT ACTIVE SITES IN PYRUVATE CARBOXYLASE

Interactions in the presence of varying concentrations of the substrates pyruvate and MgATP, as well as the essential allosteric activator, acetyl-CoA, have been previously studied kinetically, but the thermodynamic relationship between binding and turnover events at each ligand's binding site has not yet been determined. Many attempts have been made in the study of allosteric regulatory mechanisms to glean the nature and source of the allosteric effects in a structure-function relationship based primarily on the enzyme structure itself; while this approach allows quantitative analysis of the effects of allosteric ligands, it does not properly take into account the full expanse of dynamic conformations through which a particular enzyme could pass during its catalytic cycle (29). Often, analyses of allosteric behavior are model-dependent and assume that an enzyme is capable of only two distinct conformational states, as described by the Monod-Wyman-Changeaux model of allosterism: a tense (T) state in the absence of a bound effector, yielding low affinity for substrates and reduced catalytic activity, and a relaxed (R) state, which has higher substrate affinity and enhanced activity, which work in concert to regulate enzyme activity (30). However, the structure of allosteric proteins is not so static in reality. The flexibility inherent in enzyme structures produces a fluctuating population of enzymes adopting any one of a variety of conformational states, some of which represent the R and T extremes of ligand affinity and catalytic competency, but most of which exhibit any of an intermediate range of states which differ only by subtle, much smaller-scale alterations in conformation (22). Thus, allosteric linkage analysis of binding events (that is, the quantification of how one ligand binds and is productively turned over in the presence or absence of a second

ligand) reveals the importance of fluctuations in enzyme function over the emphasis on changes in global structure alone and liberates the enzyme from a regulatory model that may or may not reflect the full complexity of its mechanism in actuality (29). Allosteric linkage analysis also allows quantification of the thermodynamic coupling between multiple substrates, as well as between a substrate and an effector (31, 32).

In **Fig. 22**, the general reaction scheme of a single-substrate-single-modifier mechanism is illustrated to serve as a guide for understanding the general processes by which allosteric enzymes are regulated. The substrate, A, is capable of binding to the enzyme (E) and generating a product from the binary complex in the absence of the allosteric effector, X. However, when both A and X bind to the enzyme, the catalytic activity of the resultant ternary complex is different (either enhanced or depressed, depending on the stimulatory or inhibitory nature of the effector) than that of the binary complex. In terms of the kinetic mechanism of an enzyme, the order in which binding events occur matters; in the reaction scheme shown, the binding order of A and X influences the overall rate of the reaction. Thermodynamically, though, the interaction of an enzyme with multiple substrates to achieve a ternary or quaternary complex can occur in any order; that is, the energetic properties of the overall reaction will be equivalent, regardless of whether A or X is bound to the enzyme first (33).

Regulated activity of PC produces oxaloacetate for utilization in glucose metabolism, whether through completion of the first committed step in the gluconeogenic pathway or through anaplerosis of TCA cycle intermediates for cellular energy production, and it accomplishes this by lowering the activation energy of the conversion of pyruvate to oxaloacetate through

stabilization of the reaction's transition state. Given the activating and stabilizing effects that bound acetyl-CoA exerts on PC, and the resultant increases in BC domain activity and kinetic coupling of the BC and CT domain reactions, we have sought to determine the extent to which acetyl-CoA enhances the thermodynamic favorability of the catalyzed production of oxaloacetate by examining the activation energy of the reaction in the presence and absence of acetyl-CoA. By taking into account the emerging, more dynamic view of allostery described previously, it is possible to imagine a mechanism in which PC is better able to stabilize the transition state intermediates of each domain reaction due subtle alterations in active site chemistry or binding pocket conformation caused by the presence of acetyl-CoA, thus possibly reducing the activation energy of pyruvate carboxylation even further (4, 34, 35).

We determined the thermodynamic-linkage of each ligand of PC, using the wild-type form of PC from *S. aureus*. We have measured the initial rate of pyruvate carboxylation by varying the concentration of two ligands simultaneously, while holding the third ligand at a constant saturating concentration. It also is essential to understand each individual interaction in order to piece together the network of amino acids and subunit domains that is ultimately responsible for the allosteric response elicited upon binding of acetyl-CoA (34). The task of measuring allosteric regulation in multifunctional, multisubunit enzymes such as PC is a complex one, given that catalysis must occur intermolecularly, and that the majority of electrostatic residue interactions occurs between faces rather than within a single face. As such, the BC and CT domain active sites necessary to produce one oxaloacetate are located on two separate polypeptide chains, while binding of acetyl-CoA in its pocket formed between the allosteric domain and the BC domain is required for stimulation of the overall catalytic rate. The results obtained from our lab describing

the communication signaling mechanism between PC subunits as occurring intermolecularly within a face lend credence to a possible allosteric regulatory mechanism involving thermodynamically favorable shifts in ligand domain conformations upon binding of pyruvate, MgATP, or acetyl-CoA, and which does not necessarily rely on a physical amino acid network connecting any two of the binding sites.

In each ligand coupling interaction examined (i.e., pyruvate vs. MgATP, pyruvate vs. acetyl-CoA, and MgATP vs. acetyl-CoA), comparison of the apparent K_m at fixed-variable concentrations of one ligand for the full-forward pyruvate carboxylation reaction across increasing concentrations of a second ligand enabled us to calculate the Gibbs' free energy of each binding and catalytic turnover relationship. The ability of either MgATP or pyruvate to increase affinity of PC for the other is observed in the presence of acetyl-CoA, while this relationship is entirely lost in its absence. These results have the potential to further elucidate the nature of intersubunit communication, in that the enzyme's spatially distinct active sites, even in the presence of the preferred substrates, cannot communicate or coordinate productive catalytic coupling in the absence of the activator. We also demonstrate here that, despite acetyl-CoA's critical role in coupling the BC and CT domains, establishing the communication network necessary for pyruvate occupancy to influence BCCP domain translocation, stabilizing the tetramer, and dramatically enhancing the rate of MgATP-cleavage, its thermodynamic and regulatory contributions are not reflected in the activation energy of the enzyme.

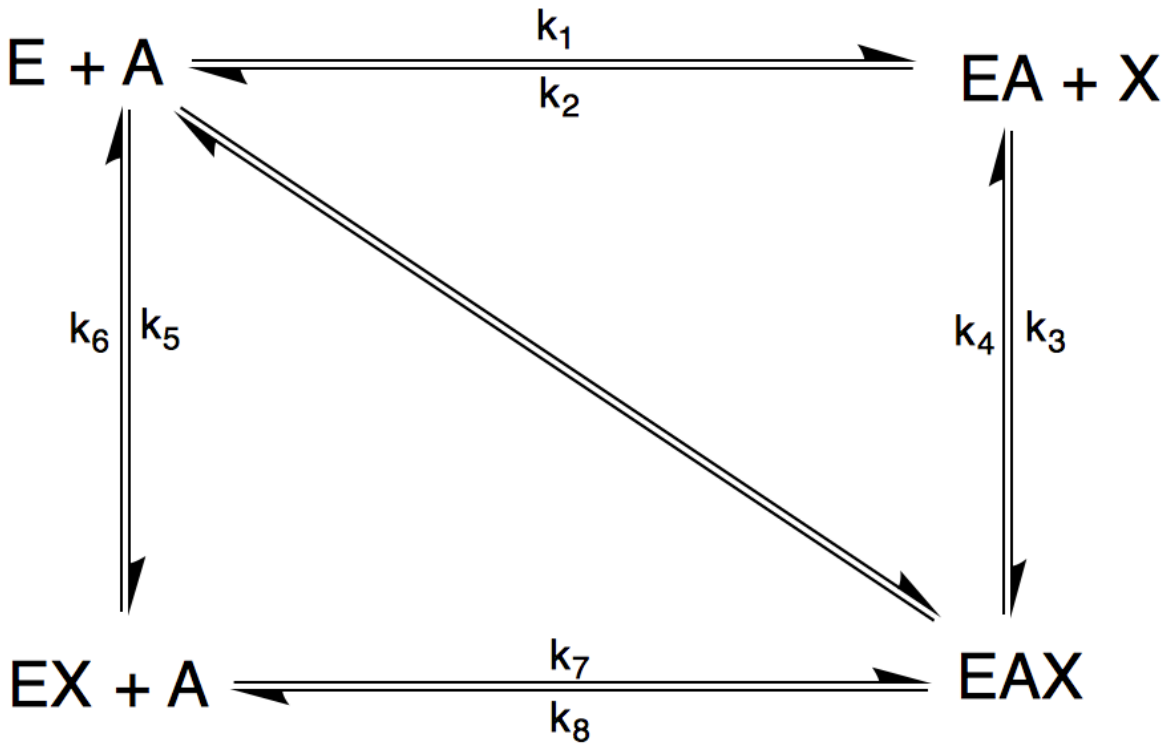

FIGURE 22. Thermodynamic reaction scheme for an enzyme (E) with one substrate (A) and one effector (X). Binding events involving both the substrate and effector are required to form the ternary complex (EAX), from which point the reaction can proceed to product formation. Each addition of a ligand, or removal of a bound ligand, is defined by its own kinetic rate constant (k_1 through k_8). Kinetically, the order in which the two ligands bind with the enzyme determines the overall rate of the reaction and is essential knowledge for understanding the catalytic mechanism of that enzyme. In terms of thermodynamics, however, the pathway between the free enzyme (E) and the fully bound ternary complex (EAX), denoted by the diagonal set of arrows, requires an equivalent amount of energy regardless of which binding event occurs first; that is, $k_1 + k_3$ is energetically equivalent to $k_5 + k_7$. In the case of PC, the complex required for catalysis involves three substrates (pyruvate, MgATP, and HCO_3^-) and one allosteric effector (acetyl-CoA), adding significant complexity to the reaction scheme.

METHODS

Plasmid expression, protein overexpression, purification, and visualization were performed as described previously (refer to Chapter 1).

Steady-State Enzyme Activity Assays

The initial rates of pyruvate carboxylation and HCO_3^- dependent MgATP-cleavage were determined spectrophotometrically using coupled assay systems. All reactions were performed at 25° C in 1 mL reaction volumes and 100 mM Tricine (pH 7.6). Assays were carried out using the Shimadzu UV-1800 Spectrophotometer, CPS-240A Cell Positioner, and 6 Cell-Thermoelectrical Temperature Controller.

Temperature Dependence of Acetyl-CoA Activation

Specific activity of pyruvate carboxylation in the presence of saturating pyruvate (15 mM) and MgATP (2.5 mM) was determined for *Sa*PC wild type across a range of temperatures (15 – 55°C) in the presence and absence of saturating acetyl-CoA (250 μM).

Thermodynamic Linkage Analysis of SaPC

The initial rates of oxaloacetate formation were measured across variable concentrations of pyruvate (0.25 – 15 mM), MgATP (0.05 – 3 mM), and acetyl-CoA (0 – 250 μM); when the concentration of one ligand was varied, the second ligand was measured at fixed variable concentrations, and the third ligand was held constant at saturating concentrations. Reactions also contained: 100 mM HCO_3^-, 5 mM $MgCl_2$, 0.25mM NADH, and malate dehydrogenase (55

units). Reactions were initiated with the addition of ~0.01 – 1.36 mg of PC. Initial velocity data were fit to equation (10).

Specific Activity in High-Viscosity Buffer

Initial velocities of oxaloacetate formation and inorganic phosphate release by wild-type *Sa*PC were determined in the presence of saturating substrates (15 mM pyruvate, 2.5 mM MgATP, and 250 μM acetyl-CoA) and increasing concentrations of selected viscosigens. Reaction buffers contained one of glycerol (0 – 60% v/v), sucrose (0 – 60% w/v), or Ficoll 400 (0 – 50% w/v). Pyruvate carboxylation and MgATP-cleavage were measured as described previously using the malate dehydrogenase and purine nucleoside phosphorylase coupled assay systems, respectively.

Data Analysis

Temperature Dependence of Acetyl-CoA Activation. Data were fit to the Arrhenius equation (equation 12a), from which the slope was used to determine the activation energy of PC's catalytic cycle (equation 12b) in the presence and absence of acetyl-CoA.

$$k = Ae^{-\frac{E_a}{RT}} \qquad (12a)$$

$$\text{Slope} = -\frac{E_a}{R} \qquad (12b)$$

Thermodynamic Linkage Analysis of SaPC. Lineweaver-Burk secondary plots of *Sa*PC thermodynamic-linkage data were generated and fit to a linear regression. The Lineweaver-Burk equation is a transformation of the Michaelis-Menten (equation 10).

$$\frac{1}{v_i} = \frac{K_{m\ pyruvate}}{V_{\max}}\left(\frac{1}{[pyruvate]}\right) + \frac{1}{V_{\max}} \qquad (13)$$

Free energy values were determined by fitting secondary plots of apparent K_m versus ligand concentration to equation (14) using nonlinear regression analysis (33). In this equation, K^o_{app} is equal to K_{app} when ligand [B] = 0, $K^o_{ix/b}$ is the dissociation constant for ligand B when ligand [A] = 0 when, $Q_{ax/b}$ is the coupling constant between ligands A and B when ligand B is at saturating concentration, and [B] is the concentration of ligand B. For these experiments, ligands A and B can represent MgATP and acetyl-CoA, pyruvate and acetyl-CoA, or MgATP and pyruvate, whereby ligand [A] is varied, ligand [B] is held at fixed-variable concentrations, and the third ligand, [C], is held at saturating concentration.

$$K_{app} = K^{\circ}_{app}\left(\frac{K^{\circ}_{ix/b} + [B]}{K^{\circ}_{ix/b} + Q_{ax/b}[B]}\right) \qquad (14)$$

The coupling constant determined in equation (14) was then used to relate the thermodynamic relationships between ligands to free energy using equation (15), in which $\Delta G_{ax/b}$ represents the coupling free energy between binding events of ligands A and B, R is the ideal gas constant (kcal mol^{-1} K^{-1}), and T is temperature (K):

$$\Delta G_{ax/b} = -RT\ln\left(Q_{ax/b}\right) \qquad (15)$$

RESULTS

Activation Energy of PC is Not Lowered in the Presence of Acetyl-CoA.

Pyruvate carboxylation activity of PC (k_{cat}) was determined using the malate dehydrogenase coupled assay system to indirectly measure oxaloacetate formation, as described previously. This was carried out across a broad range of temperatures (15-55°C) in order to determine the activation energy of catalysis in the presence or absence of acetyl-CoA (**Fig. 23**). Given the structural importance of acetyl-CoA in promoting tetramerization and stabilizing the allosteric domain, we made the initial assumption that the presence of acetyl-CoA in the allosteric domain would lower the activation energy of PC-catalyzed carboxylation of pyruvate. Specific activities of pyruvate carboxylation at each temperature were analyzed as a function of inverse temperature (K^{-1}) (eqn 12a). In the presence of acetyl-CoA, the slope, which is $-E_a/R$, was -8160 ± 290 K^{-1}, and the corresponding activation energy was 16.2 ± 0.7 kcal mol^{-1}. In the absence of acetyl-CoA, this slope was -8560 ± 310 K^{-1}, which corresponded to an activation energy of 17.0 ± 0.6 kcal mol^{-1}. Thus, the presence or absence of acetyl-CoA in the allosteric domain did not significantly alter the activation energy of catalysis for PC.

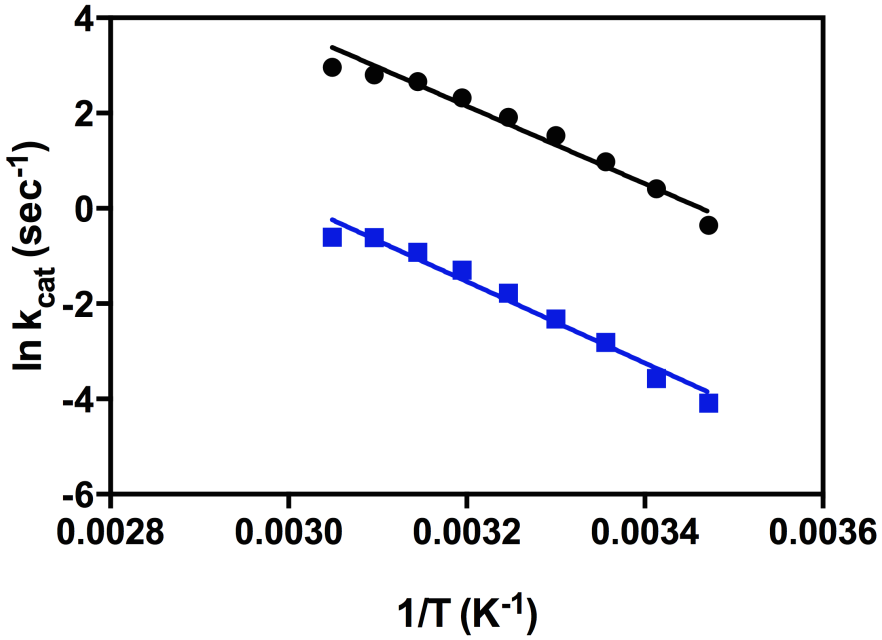

FIGURE 23. Arrhenius plot demonstrating activation energy of PC in the presence (●) and absence (■) of acetyl-CoA. Initial rate is shown as a function of inverse temperature (K^{-1}). Slope of each line represents $-E_a/R$, in which E_a is the activation energy of catalysis for PC and R is the ideal gas constant (1.986×10^{-3} kcal K^{-1} mol^{-1}).

Rates of Pyruvate Carboxylation at Varying Ligand Concentrations.

The k_{cat} (sec^{-1}) of pyruvate carboxylation was determined by measuring initial rates of oxaloacetate formation for the wild-type form of *Sa*PC. Concentrations of pyruvate (0.25–15 mM), MgATP (0.05–2.5 mM), and acetyl-CoA (0–250 μM) were individually manipulated to examine oxaloacetate formation as a function of the binding and catalytic turnover relationship between pyruvate and acetyl-CoA, MgATP and acetyl-CoA, and pyruvate and MgATP. For each pair of ligands examined, the concentration of the third was held constant at saturating levels. All rates exhibited Michaelis-Menten type responses as substrate concentrations were increased, and the fixed-variable concentrations of each ligand yielded both V-type and K-type effects on the rate of oxaloacetate production.

Pyruvate carboxylation activity in the presence of varying concentrations of pyruvate and acetyl-CoA (**Fig. 25**, A), as well as a constant, saturating MgATP concentration of 2.5 mM, exhibited a 72-fold increase in the k_{cat} between the absence (0.033 ± 0.002 s^{-1}) and saturating presence (2.38 ± 0.05 s^{-1}) of acetyl-CoA at 15 mM pyruvate (**Table 7**). The apparent $K_{m\ pyruvate}$ was determined to be 0.47 ± 0.05 mM in the presence of saturating acetyl-CoA, which was approximately 4-fold lower than the apparent $K_{m\ pyruvate}$ at 7 μM acetyl-CoA (1.9 ± 0.3 mM). When MgATP and acetyl-CoA concentrations were varied (**Fig. 24**), while pyruvate was held constant at 15 mM, a similar V-type effect was observed between the absence (0.037 ± 0.004 sec^{-1}) and presence of saturating acetyl-CoA (2.55 ± 0.04 sec^{-1}) at saturating MgATP. The apparent $K_{m\ MgATP}$ was modestly affected by increasing concentrations of acetyl-CoA, measuring 0.22 ± 0.04 mM at saturating acetyl-CoA compared to 0.6 ± 0.2 mM in the absence of acetyl-CoA (**Table 6**). Finally, when concentrations of pyruvate and MgATP were varied in the presence of saturating

acetyl-CoA (**Fig. 26**), a 3.7-fold decrease in k_{cat} and a 3.3-fold increase in $K_{m\ pyruvate}$ was observed between the presence of saturating (2.5 mM) and subsaturating (0.05 mM) concentrations of MgATP (**Table 8**).

It has been demonstrated that PC catalyzes the formation of oxaloacetate through a bi bi uni uni nonclassical ping-pong mechanism (36, 37), meaning that the first two substrates (MgATP and HCO_3^-) bind to the BC domain and are converted to two released products (MgADP and P_i) prior to binding of the single substrate (pyruvate) to the CT domain active site and conversion to a single product (oxaloacetate). We sought to hone this mechanism further by examining the binding and turnover relationship between each pair of varied ligands (MgATP and acetyl-CoA, pyruvate and acetyl-CoA, and pyruvate and MgATP) through generation of double-reciprocal plots (**Fig. 24-26**, B) using equation (13). Generally, a Lineweaver-Burk plot of an enzyme following a classical ping-pong mechanism will yield a series of parallel lines at varying concentrations of the effector, while an enzyme controlled by a sequential mechanism will produce a Lineweaver-Burk plot with intersecting lines at varying effector concentrations. Each of the three ligand binding relationships examined yielded double reciprocal plots with intersecting lines, with both slope (**Fig. 24-25,** C) and y-intercept (**Fig. 24-25**, D) increasing as the effector concentration decreased. This pattern is suggestive of a random sequential enzyme mechanism under rapid equilibrium, whereby occupancy of both ligands in their respective, spatially discrete binding sites is necessary in order for pyruvate carboxylation activity to proceed.

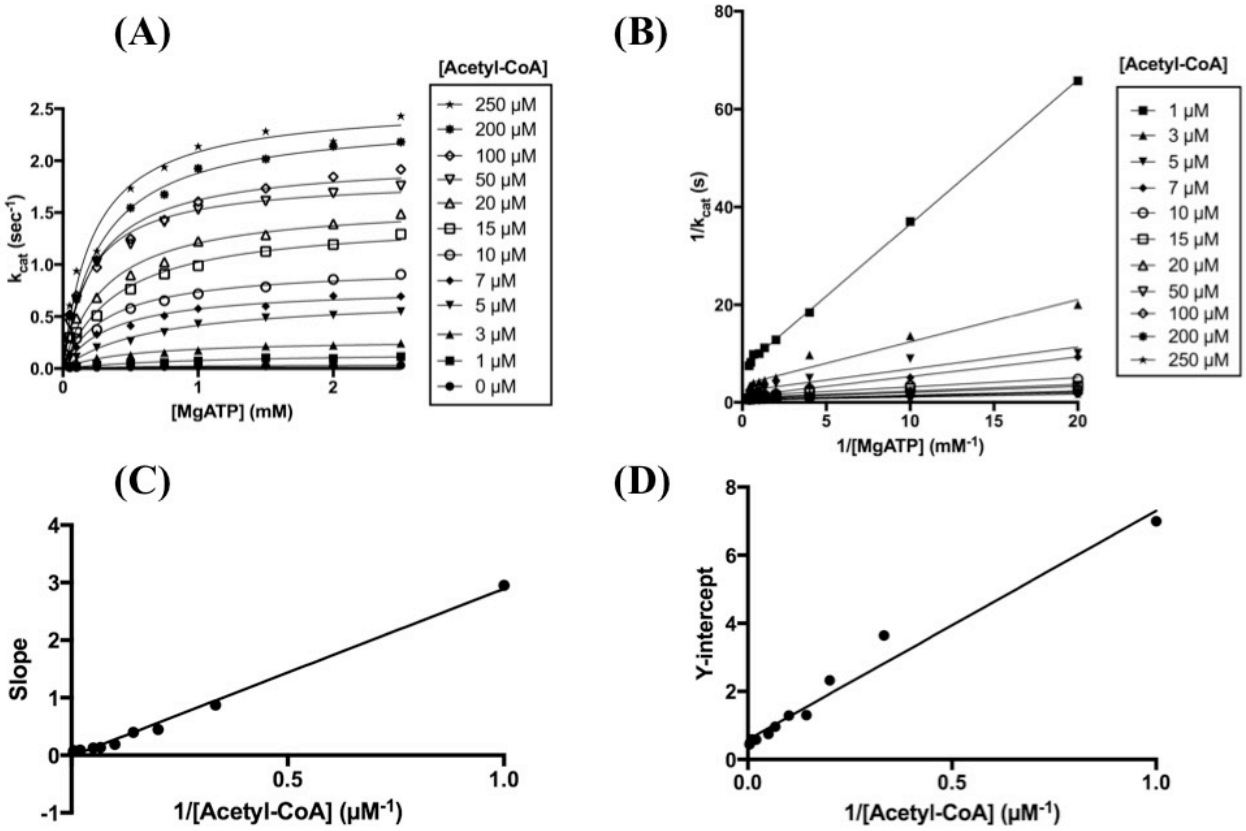

FIGURE 24. *(A)* The initial rate of oxaloacetate formation by *Sa*PC, in k_{cat} (s^{-1}), measured as a function of increasing MgATP concentration. MgATP is measured at varying concentrations (0 – 3 mM) in the presence of saturating pyruvate (15 mM) at fixed-variable concentrations of acetyl-CoA (0 – 250 µM). *(B)* Lineweaver-Burk double reciprocal plot of initial rates of pyruvate carboxylation. Inverse rate is represented as a function of the inverse concentration of MgATP. *C-D:* Secondary plots analyzing the slope (*C*) and y-intercept (*D*) of linear regression lines from the Lineweaver-Burk plot, represented as a function of the inverse concentration of acetyl-CoA.

[Acetyl-CoA] (μM)	k_{cat} (s^{-1})	$K_{m\ MgATP}$ (mM)
0	0.038 ± 0.004	0.6 ± 0.2
1	0.149 ± 0.007	0.47 ± 0.07
3	0.37 ± 0.02	0.52 ± 0.09
5	0.68 ± 0.04	0.7 ± 0.1
7	0.87 ± 0.02	0.44 ± 0.04
10	0.98 ± 0.05	0.33 ± 0.06
15	1.44 ± 0.08	0.40 ± 0.07
20	1.59 ± 0.08	0.32 ± 0.06
50	1.83 ± 0.05	0.20 ± 0.02
100	2.00 ± 0.09	0.24 ± 0.04
200	2.41 ± 0.07	0.28 ± 0.03
250	2.6 ± 0.1	0.22 ± 0.04

TABLE 6. Initial rate measurement of pyruvate carboxylation at variable concentrations of MgATP, fixed-variable concentrations of acetyl-CoA, 15 mM pyruvate, and 100 mM HCO_3^-.

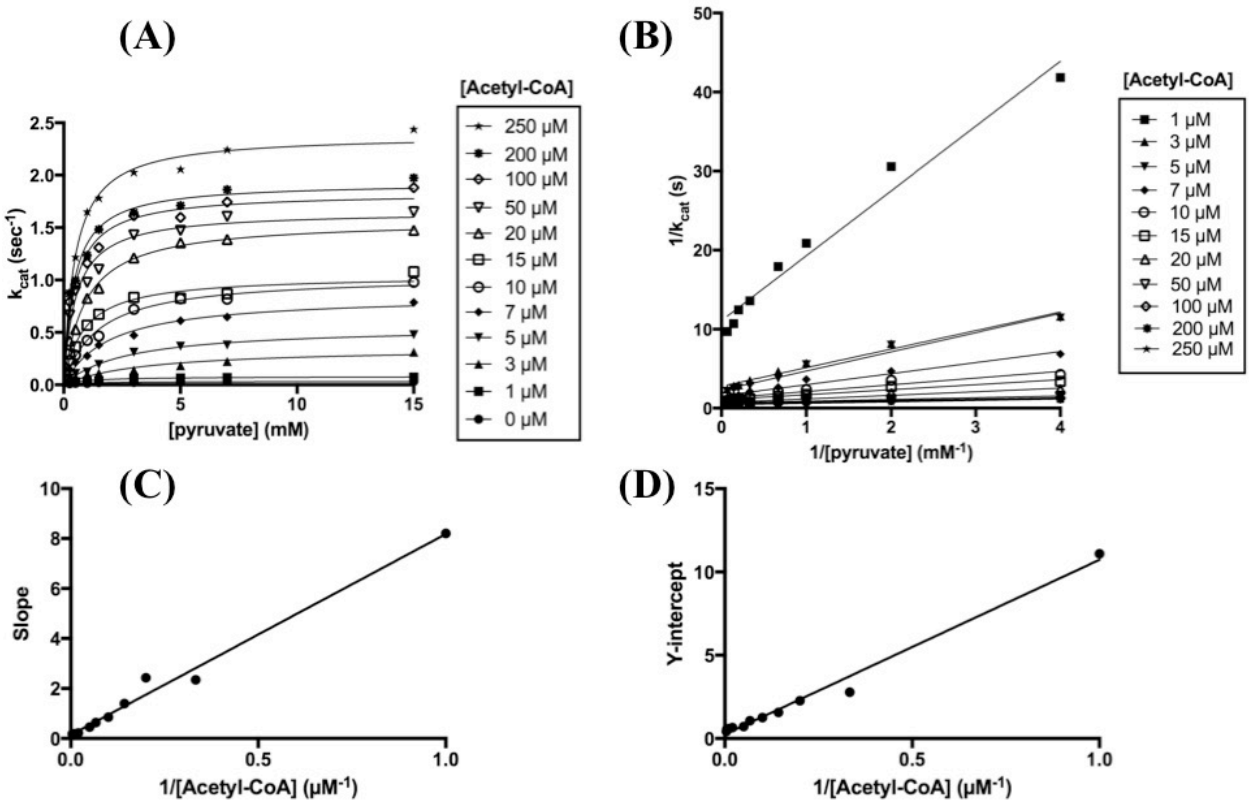

FIGURE 25. *(A)* The initial rate of oxaloacetate formation by *Sa*PC, in k_{cat} (s^{-1}), measured as a function of increasing pyruvate concentration. Pyruvate is measured at varying concentrations (0 – 15 mM) in the presence of saturating MgATP (2.5 mM) at fixed-variable concentrations of acetyl-CoA (0 – 250 µM). *(B)* Lineweaver-Burk double reciprocal plot of initial rates of pyruvate carboxylation. Inverse rate is represented as a function of the inverse concentration of pyruvate. *C-D:* Secondary plots analyzing the slope (*C*) and y-intercept (*D*) of linear regression lines from the Lineweaver-Burk plot, represented as a function of the inverse concentration of acetyl-CoA.

[Acetyl-CoA] (μM)	k_{cat} (s^{-1})	$K_{m\ pyruvate}$ (mM)
0	0.033 ± 0.002	0.9 ± 0.2
1	0.108 ± 0.004	1.3 ± 0.2
3	0.44 ± 0.01	1.5 ± 0.2
5	0.52 ± 0.01	1.5 ± 0.1
7	0.85 ± 0.04	1.9 ± 0.3
10	1.04 ± 0.05	1.4 ± 0.2
15	1.04 ± 0.05	0.8 ± 0.2
20	1.57 ± 0.04	0.91 ± 0.08
50	1.65 ± 0.07	0.51 ± 0.09
100	1.83 ± 0.06	0.46 ± 0.08
200	1.93 ± 0.07	0.43 ± 0.07
250	2.38 ± 0.05	0.47 ± 0.05

TABLE 7. Initial rate measurement of pyruvate carboxylation at variable concentrations of pyruvate, fixed-variable concentrations of acetyl-CoA, 2.5 mM MgATP, and 100 mM HCO_3^-.

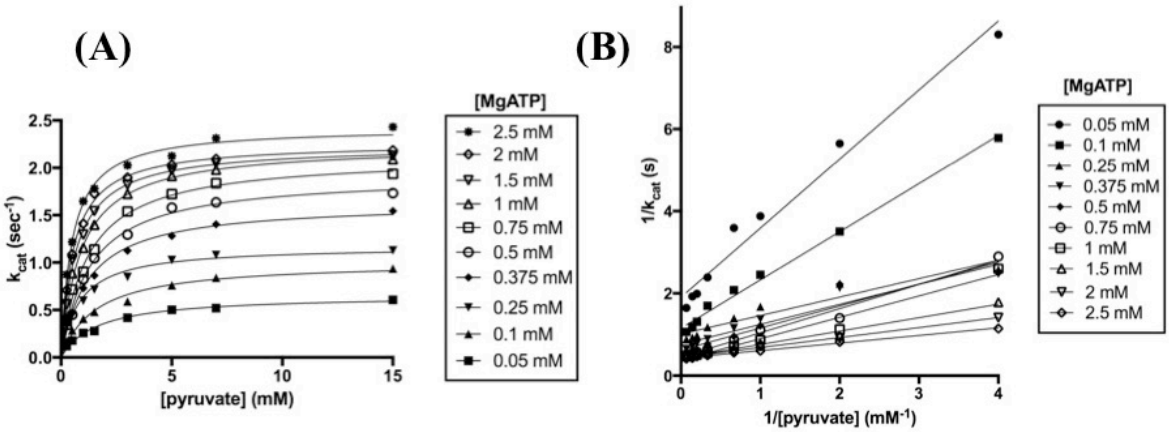

FIGURE 26. *(A)* The initial rate of oxaloacetate formation by *Sa*PC, in k_{cat} (s^{-1}), measured as a function of increasing pyruvate concentration. Pyruvate is measured at varying concentrations (0 – 15 mM) in the presence of saturating acetyl-CoA (250 μM) at fixed-variable concentrations of MgATP (0 – 2.5 mM). *(B)* Lineweaver-Burk double reciprocal plot of initial rates of pyruvate carboxylation. Inverse rate is represented as a function of the inverse concentration of pyruvate.

[MgATP] (mM)	k_{cat} (s^{-1})	$K_{m\ pyruvate}$ (mM)
0.05	0.66 ± 0.03	1.6 ± 0.2
0.1	1.01 ± 0.04	1.6 ± 0.2
0.25	1.17 ± 0.05	0.8 ± 0.1
0.5	1.92 ± 0.06	1.3 ± 0.1
0.75	2.12 ± 0.05	1.21 ± 0.09
1	2.24 ± 0.05	0.90 ± 0.07
1.5	2.23 ± 0.03	0.67 ± 0.04
2	2.26 ± 0.03	0.55 ± 0.03
2.5	2.42 ± 0.04	0.49 ± 0.04

TABLE 8. Initial rate measurements of pyruvate carboxylation at variable concentrations of pyruvate, fixed-variable concentrations of MgATP, 250 μM acetyl-CoA, and 100 mM HCO_3^-.

Thermodynamic Linkage Analysis of Acetyl-CoA and Substrates.

In order to identify whether the energetic coupling of interactions in the BC, CT, and allosteric domains contributes to regulation of PC's catalytic mechanism, we also examined the energetic coupling of binding and catalytic turnover between pyruvate, MgATP, and acetyl-CoA. The initial rates of oxaloacetate formation were measured as described previously at variable concentrations of pyruvate and MgATP, each with fixed-variable concentrations of acetyl-CoA and saturating concentrations of the third ligand, and apparent $K_{m\ pyruvate}$ and apparent $K_{m\ MgATP}$ were determined between the absence and saturating presence of acetyl-CoA (**Fig. 27**). The data were fit to equation (14), which relates the apparent K_m of a substrate in the presence and absence of a bound activator. As the allosteric activator concentration was varied, the $K_{m\ pyruvate}$ fell from 1.6 ± 0.1 mM at 0 μM acetyl-CoA to 0.5 ± 0.1 mM at 250 μM acetyl-CoA, reflecting a 3.2-fold increase in the affinity of the enzyme for pyruvate binding as saturation of acetyl-CoA was reached. The apparent $K_{m\ MgATP}$ followed a similar pattern with a 2.2-fold decrease in MgATP binding affinity, being the highest in the absence of acetyl-CoA (0.53 ± 0.07 mM) and the lowest in its saturating presence (0.24 ± 0.05 mM).

From the maximum and minimum apparent K_m for pyruvate and MgATP, we then determined the apparent free energy coupling constant (Q_{ax}), which was described in equation (14), for each substrate (**Table 9**). This term allowed us to quantitatively describe the thermodynamic consequences on substrate binding and turnover in the reaction mechanism of PC due to the concentration of the allosteric activator (29). Q_{ax} was calculated as the quotient of the apparent K_m of each substrate in the absence of the activator and the apparent K_m in the saturating presence of the activator. In order to determine the thermodynamic coupling of catalysis between

binding of ligands at spatially separate active sites, the Q_{ax} value for each ligand binding relationship was then substituted into equation (15) to calculate the Gibbs' free energy value of coupling (**Table 10**). The Gibbs' free energy of coupling between pyruvate and acetyl-CoA was calculated to be -0.65 ± 0.09 kcal mol^{-1}, while the value for the relationship between MgATP and acetyl-CoA was about 28% lower in magnitude (-0.47 ± 0.08 kcal mol^{-1}).

Thermodynamic Linkage Analysis of Pyruvate and MgATP

By comparing the binding and turnover of either pyruvate or MgATP to acetyl-CoA binding, we have been able to determine that acetyl-CoA directly affects the ability of PC to bind either substrate, though it more dramatically influences the binding and catalytic turnover of pyruvate in the CT domain. However, we also were interested to investigate whether MgATP or pyruvate occupancy in their respective domain active sites thermodynamically affected the binding of one another (**Fig. 28**). We have examined the relationship between MgATP binding in the BC domain and pyruvate binding in the CT domain, both in the presence and absence of saturating acetyl-CoA bound in the allosteric domain, and calculated the apparent $K_{m,\ pyruvate}$ across increasing concentrations of MgATP.

Initial rates of oxaloacetate formation were measured as described previously, varying pyruvate between 0.25 – 15 mM and MgATP between 0.1 – 3 mM, at 0 μM and 250 μM acetyl-CoA. The apparent $K_{m\ pyruvate}$ in the presence of acetyl-CoA was the highest at low concentrations of MgATP (1.6 ± 0.2 mM), steadily decreasing as MgATP concentrations were raised to saturating (2.5 mM) to achieve a minimum apparent $K_{m\ pyruvate}$ of 0.49 ± 0.04 mM, a 3.3-fold increase in binding affinity. The initial rate was also measured at 3 mM MgATP, which is supersaturating,

and significant substrate inhibition of oxaloacetate formation, along with an increase in the $K_{m\ pyruvate}$ to 0.8 ± 0.2 mM, was observed as expected. Substrate inhibition at high MgATP concentrations is likely due to nonproductive binding in the BC domain, possibly because of several MgATP molecules attempting to access a single active site simultaneously.[48] Interestingly, in the absence of acetyl-CoA, the apparent $K_{m\ pyruvate}$ remained constant, at 1.7 ± 0.3 mM, regardless of the concentration of MgATP.

The thermodynamic coupling constant, Q_{ax}, was again calculated from the determined apparent $K_{m\ pyruvate}$ values (**Table 9**). At 250 μM acetyl-CoA, a Q_{ax} value of 2.5 ± 0.2 was calculated, while at 0 μM acetyl-CoA, the invariance of $K_{m\ pyruvate}$ across saturating and subsaturating concentrations of MgATP resulted in a coupling constant of 1.0 ± 0.2. Substituting the coupling constants again into equation (15), we were able to calculate the Gibbs' free energy of coupling between pyruvate and MgATP with and without the aid of the allosteric activator (**Table 10**). ΔG in the presence of acetyl-CoA was determined to be -0.5 ± 0.1 kcal mol^{-1}, suggesting that either pyruvate or MgATP occupancy in the CT or BC domain binding pockets, respectively, elicits thermodynamic consequences on the binding of the other when acetyl-CoA is present to facilitate catalysis. However, when acetyl-CoA is not present in the allosteric domain, the Gibbs' free energy of coupling is 0 kcal mol^{-1}, which indicates a complete absence of thermodynamic-linkage between the BC and CT domain active sites on the same monomer.

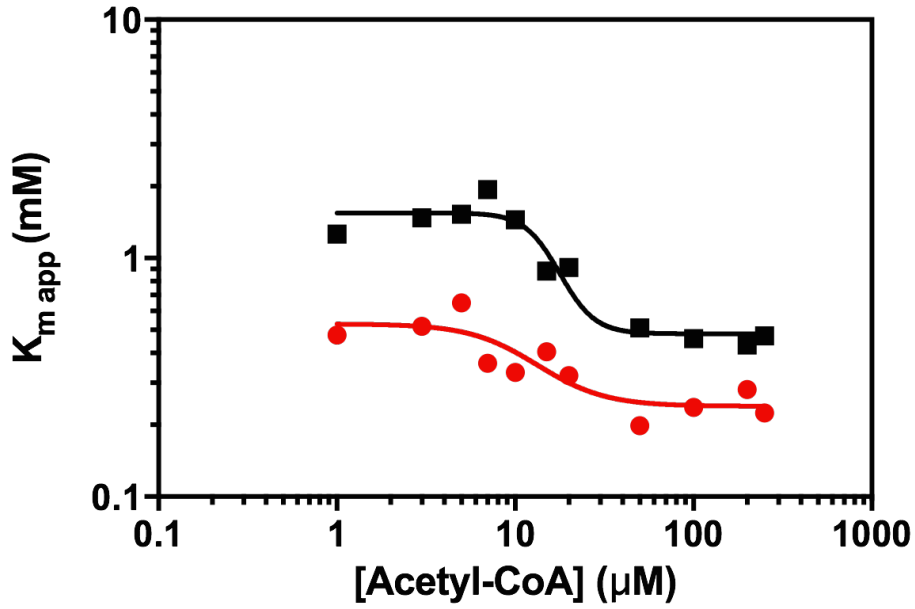

FIGURE 27. Apparent $K_{m\ pyruvate}$ (■) and $K_{m\ MgATP}$ (●) plotted as a function of increasing concentrations of acetyl-CoA.

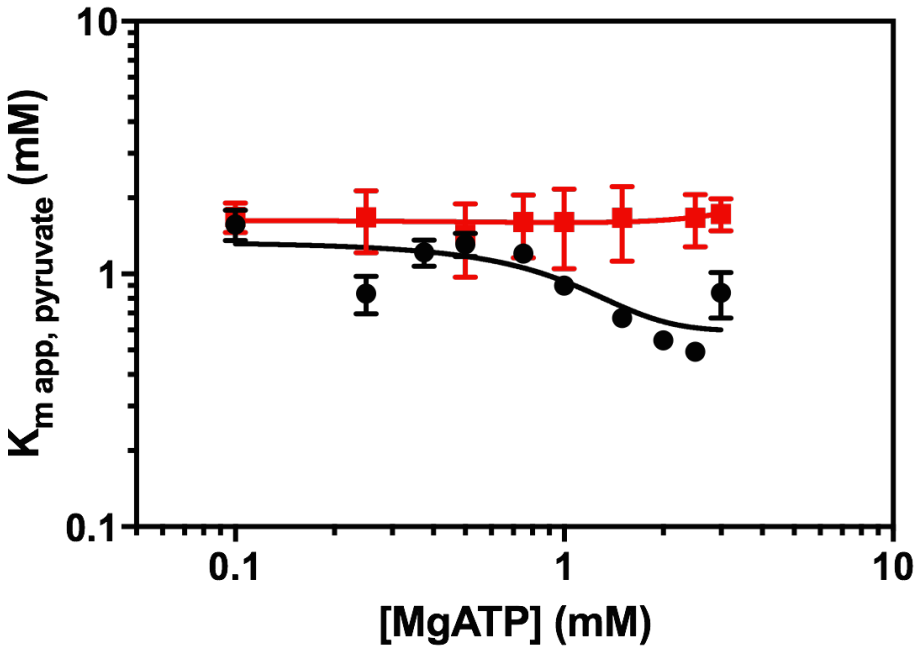

FIGURE 28. Apparent $K_{m\ pyruvate}$ as a function of increasing concentrations of MgATP. The thermodynamic relationship between pyruvate and MgATP is shown both in the presence of 250 µM (●) and 0 µM (■) acetyl-CoA. The increase in $K_{app\ pyruvate}$ in the presence of acetyl-CoA is due to substrate inhibition that occurs above saturating concentrations of MgATP (> 2.5 mM).

	K_{ia}^{o} (mM)	K_{ia}^{∞} (mM)	Q_{ax}
Pyruvate vs. Acetyl-CoA	1.5 ± 0.1	0.5 ± 0.1	3 ± 0.1
MgATP vs. Acetyl-CoA	0.53 ± 0.07	0.24 ± 0.05	2.208 ± 0.06
Pyruvate vs. MgATP, 250 µM Acetyl-CoA	1.5 ± 0.3	0.6 ± 0.1	2.5 ± 0.2
Pyruvate vs. MgATP, 0 µM Acetyl-CoA	1.7 ± 0.3	1.7 ± 0.2	1.0 ± 0.2

TABLE 9. Determination of the free energy coupling constant, Q_{ax}, from initial rates of oxaloacetate formation measured with each combination variable-concentration ligands. K_{ia}^{o} represents the apparent K_m of the first listed ligand (of each pair) in the absence of the second listed ligand, while K_{ia}^{∞} represents the apparent K_m of the first ligand in the saturating presence of the second ligand. Q_{ax} is the quotient of these two values.

	Q_{ax}	ΔG (kcal mol^{-1})
Pyruvate vs. Acetyl-CoA	3 ± 0.1	-0.65 ± 0.09
MgATP vs. Acetyl-CoA	2.21 ± 0.06	-0.47 ± 0.08
Pyruvate vs. MgATP, 250 µM Acetyl-CoA	2.5 ± 0.2	-0.5 ± 0.1
Pyruvate vs. MgATP, 0 µM Acetyl-CoA	1.0 ± 0.2	0.0 ± 0.0

TABLE 10. Gibbs' free energy of coupling determined from initial rates of oxaloacetate concentration across varying concentrations of substrates, pyruvate and MgATP, and the allosteric activator, acetyl-CoA. Q_{ax} values determined for each ligand pair examined were substituted into equation (15), at 298 K and with an ideal gas constant (R) of 1.985×10^{-3} kcal K^{-1} mol^{-1}, to calculate the thermodynamic binding and turnover relationship between the binding sites of each ligand.

Pyruvate Carboxylation as a Function of Solution Viscosity.

The initial rate (s^{-1}) of pyruvate carboxylation was determined for wild-type *Sa*PC in solutions of increasing viscosity using either glycerol (0 – 60% v/v), sucrose (0 – 60% w/v), or Ficoll PM 400, which is a 400 kDa polymer of sucrose and epichlorohydrin (0 – 40% w/v) (**Fig. 29**). In all three cases, the initial velocity in the presence of saturating substrates increased at low viscosity, peaking at 25% glycerol (1.095 μmol min^{-1} mg^{-1}), 10% sucrose (1.026 μmol min^{-1} mg^{-1}), and 5% Ficoll PM 400 (0.908 μmol min^{-1} mg^{-1}); after these points, the rate of catalysis decreased linearly with respect to increasing percentage of viscosigen in solution. Glycerol had the greatest suppressive effect on the rate of pyruvate carboxylation, with the slope of the rate decrease following 25% glycerol being -0.031 ± 0.002 μmol min^{-1} mg^{-1} $(\text{percent glycerol})^{-1}$; sucrose had the least effect on the rate, with a rate of decrease of -0.0168 ± 0.0006, and Ficoll had an intermediate effect (-0.021 ± 0.002).

Calculated viscosities of glycerol, sucrose, and Ficoll solutions at 25ºC, at which our rate measurements were recorded, have been published in the literature, and offer some insight into the rate at which each solution depresses the specific activity of PC (**Fig. 29; Table 11**). Glycerol is the smallest (92.1 g/mol) and least viscous of the three viscosigen molecules, reaching only 8.8 cP at 60% w/v, the maximum concentration used in this study. Sucrose is considerably larger (342.3 g/mol) and creates a significantly more viscous solution than glycerol at the same percent (w/v) concentration. Ficoll 400, as its name suggests, has a molecular weight of 400 kDa, and while it is relatively similar in size to sucrose, it maintains a highly branched, mesh-like structure in solution which yields a dramatically higher viscosity than sucrose does at the same percent

concentration. Ficoll could only be measured to 40% (w/v), due to the solution becoming so viscous beyond that point that the resulting initial rates were indistinguishable.

In the case of all three viscosigens, an initial increase in the rate of pyruvate carboxylation was observed as lower percent concentrations (less than 25% w/v) were introduced into the reaction buffer, and was eventually followed by a linear decrease in the rate as the percent of each viscosigen in solution was further elevated. There are several possible explanations that could account for this initial rise in the rate of oxaloacetate formation. One of the most likely is that, given the flexibility and general disorder of the BCCP domain inherent to the functionality of a swinging arm domain, introducing a low concentration of a viscosigen could minimize "wobbling" of the domain as it translocates back and forth within a face of the tetramer without causing a significant enough frictional force to hinder the rate of arm translocation. If this were the case, the low percentage of viscosigen in solution would be prohibiting the BCCP domain from deviating away from its optimal binding positions in either the BC or CT domains, thus enhancing the rate of catalysis. Another possibility relates to the concentration-dependent nature of PC tetramerization: since PC dissociation into monomers tends to occur at concentrations below 2 mg/mL, it is imperative that the enzyme be maintained in a high enough concentration for catalysis to occur reliably. By introducing additional molecules into the reaction buffer, it is possible that the enhanced specific activity at low percentages of glycerol, sucrose, and Ficoll 400 is due to a greater proportion of the monomers in solution being pushed together, thus promoting greater tetramerization in the slightly more viscous solution than in a buffer equivalent to water in terms of viscosity.

% Viscosigen	Viscosity (cP)		
	Glycerol	**Sucrose**	**Ficoll 400**
0	0.893	0.893	0.893
5	1.010	—	—
10	1.153	1.130	3.900
15	1.331	—	7.500
20	1.542	1.695	14.200
25	1.810	2.118	26.800
30	2.157	2.735	—
35	2.600	3.670	—
40	3.181	5.164	—
50	5.041	12.40	—
60	8.823	44.03	—

TABLE 11. Solution viscosity at 25ºC containing increasing percentages (by volume) of glycerol (38), sucrose (39, 40), or Ficoll 400 (41). Units are Centipoises, which are equivalent to mPa•s.

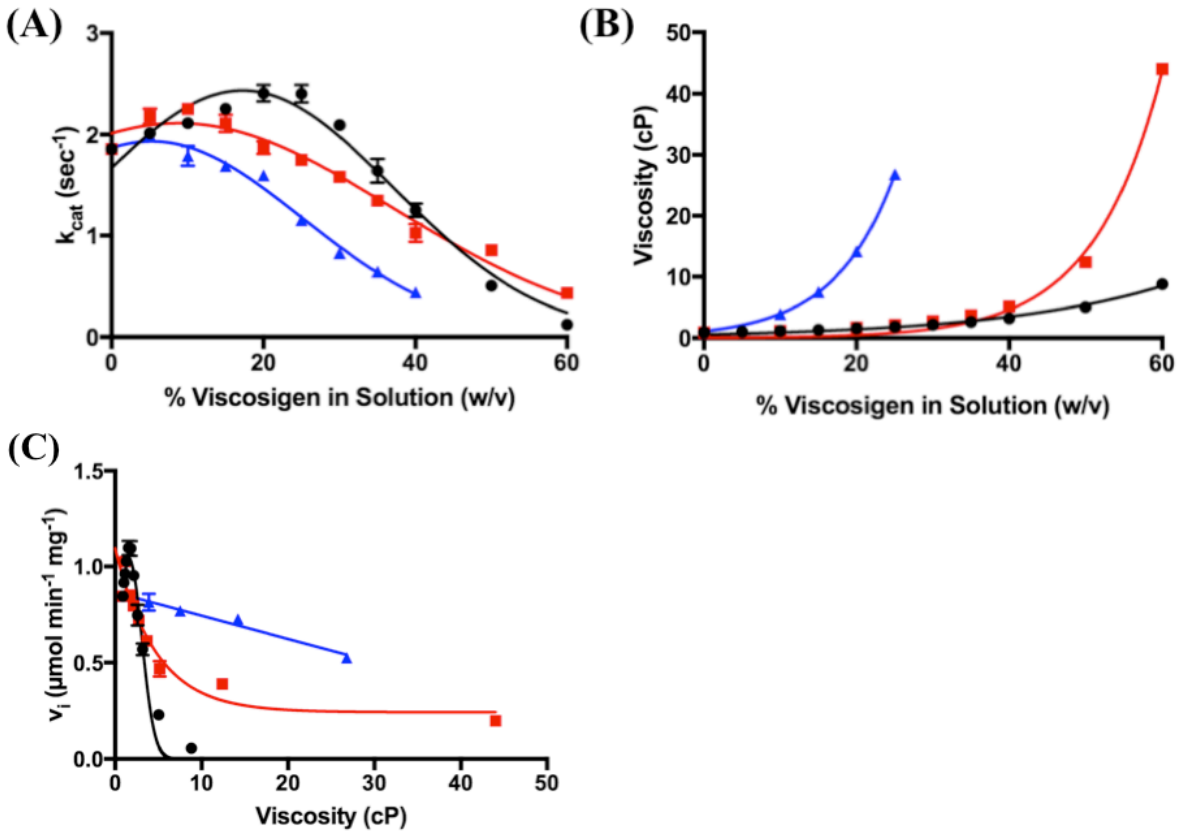

FIGURE 29. (A) k_{cat} of the full-forward pyruvate carboxylation reaction of *Sa*PC wild-type in the presence of increasing percentages of glycerol (●), sucrose (■), or Ficoll 400 (▲) dissolved in solution. (B) Viscosity, in cP, of glycerol (●), sucrose (■), and Ficoll 400 (▲) solutions from the literature. Values are shown in **Table 11**. (C) Specific activity (µmol min^{-1} mg^{-1}) of pyruvate carboxylation as a function of the viscosity of solutions containing glycerol (●), sucrose (■), or Ficoll 400 (▲).

DISCUSSION

Acetyl-CoA has already been shown to play an integral role in allosteric regulation of the kinetic mechanism of PC, positively influencing formation and maintenance of the catalytically active, tetrameric structure while also enhancing the rate of both half-reactions in the catalytic cycle. Our results, presented here, show that the presence of acetyl-CoA in the allosteric domain increases PC's affinity for both pyruvate and MgATP, though it thermodynamically affects the affinity for pyruvate to a greater extent than for MgATP. This is evident through determination of the Gibbs' free energies of coupling between pyruvate and acetyl-CoA, as well as between MgATP and acetyl-CoA. This was surprising, given the essential role of acetyl-CoA in allosteric activation of oxaloacetate formation and its role in stabilizing PC as a tetramer, and we had anticipated that its presence would enhance the reduction in activation energy for catalysis. These data suggest that, while acetyl-CoA does promote formation of oxaloacetate through allosteric activation of the enzyme and contribution of structural stability to the PC tetramer, its presence does not play a role in chemically altering the BC or CT domain active sites, thereby not further enhancing the thermodynamic favorability of the catalyzed production of oxaloacetate inherent to PC.

We did not anticipate that the presence of acetyl-CoA bound in the allosteric domain would have a more dramatic effect on pyruvate carboxylation than on MgATP-cleavage, because it has been demonstrated previously that acetyl-CoA binding asserts a greater stimulatory kinetic effect on reactions occurring in the BC domain than on those occurring in the CT domain (4, 35). Additionally, from a structural perspective, it would have seemed more plausible to assume that

acetyl-CoA would have a greater thermodynamic influence on MgATP-cleavage than on pyruvate carboxylation because of the location of its binding site: in crystal structures of PC, the effector is housed in a binding pocket formed largely between the allosteric domain and interactions with the BC domain, while minimal contact with the CT domain is made comparatively. These results suggest that CT domain occupancy by pyruvate has a greater influence on the thermodynamic forces underlying allosteric regulation by acetyl-CoA than does the MgATP-cleavage event occurring in the BC domain. When taken with the previous finding that pyruvate binding in the CT domain is essential in order to prompt BCCP—biotin release from the BC domain, it is possible to envision that the enthalpy and/or entropy associated with acetyl-CoA binding is propagated throughout the conformational ensemble to promote pyruvate binding in the CT domain as the thermodynamically favorable driving force behind the catalytic mechanism of PC.

Our data also show that acetyl-CoA, as the essential allosteric activator for PC, is responsible for mediating the thermodynamic-linkage between MgATP and pyruvate binding events in their spatially distinct active sites. The ability of either MgATP or pyruvate to increase affinity of PC for the other is observed in the presence of acetyl-CoA, while this relationship is entirely lost in its absence. Acetyl-CoA binding may possibly facilitate the correct position of the tethered biotin cofactor in the BC domain binding pocket such that it can interact with Arg353 (in *Re*PC sequence numbering), the BC domain residue responsible for biotin enolization, as well as position Arg353 such that it is capable of forming a salt bridge in order to obstruct the binding pocket, prevent reentry of carboxybiotin, and reduce the incidence of abortive decarboxylation. These results carry important implications for the nature of communication during catalysis

between the active sites within a single polypeptide chain, within a single face, and throughout the enzyme tetramer, in that the binding pockets of the enzyme's spatially distinct active sites, even in the presence of the preferred substrates, are incapable of communicating with one another to facilitate catalysis in the absence of the allosteric activator. This also supports the current view that acetyl-CoA binding somehow activates the enzyme through induction of a series of subtle conformational shifts in the overall tetrameric architecture, and could promote conformations within either or both of the BC and CT domain binding pockets to render binding and turnover thermodynamically favorable.

By studying the behavior of PC in elevated-viscosity reaction buffer, we have been able to gain valuable insight not only into the nature of the BCCP translocation step of the catalytic cycle as partially rate-limiting, but into the physiological milieu in which PC occurs naturally. Intracellular environments are highly crowded by dissolved substrates, macromolecules, cytoskeletal components, and organelle structures, rendering the cytosolic fluid much more viscous than pure water (42). Several research groups have analyzed the viscosity of cytosol through use of rotational mobility measurements (43), NMR relaxation times (44), and parallel-acquisition Fourier transform microfluorimetry in conjunction with small-molecule fluorophores (45), and all yielded average measurements between 1.0 – 3.0 cP, depending on the cell type and relative location in the cytosol from which measurements were taken (i.e., near the plasma membrane versus nearer to the cell's center). In this study, initial rates of pyruvate carboxylation peaked at approximately 25% glycerol, 10% sucrose, and 5% Ficoll, which yield solution viscosities of 1.81, 1.13, and ~2 cP, respectively. The fact that the maximal specific activities of pyruvate carboxylation for all three viscosigens occurred within the estimated viscosity range of

the cytosol of intact cells suggests that the relative crowding of PC monomers together due to the presence of countless other proteins, solutes, and macromolecules in the cytosol serves to promote localized “pockets” of concentrated PC that promotes tetramerization and stabilizes the structure to enhance its catalytic activity.

CONCLUSIONS

Through generation of functional hybrid tetramers using mutant forms of PC, we have begun to address the method by which spatially separate domains within the tetramer sense pyruvate occupancy in the CT domain. The hybrid tetramer's low apparent $K_{a\ pyruvate}$ relative to the T882S homotetramer and its loss of domain coupling, relative to the complete domain coupling observed in both the wild-type and the T882S homotetramer, indicate a signaling mechanism that is intermolecular in nature, whereby pyruvate binding to one CT domain within a face of the PC tetramer signals BCCP domain translocation on the opposing polypeptide chain. The fact that this mechanism of intersubunit signaling appears to be intermolecular in nature is suggestive that communication between spatially distinct active active sites is more complex than we had initially anticipated, and that there are likely significant thermodynamic, structural, and kinetic components to the exact nature of this mechanism. The fact that the binding pockets of the enzyme's active sites, even in the presence of their preferred substrates, are incapable of communicating with one another to facilitate catalysis in the absence of the allosteric activator strongly supports the assumption that coordination of catalysis in PC is substantially driven by thermodynamic linkages between the substrates, and between each substrate and acetyl-CoA. Our results also support the possibility of acetyl-CoA binding structurally driving the coordination of intersubunit communication through of a series of small conformational shifts in the overall tetrameric architecture.

From here, our lab will aim to examine these substrate-activator relationships further, with the goal of gaining greater understanding of the exact nature of acetyl-CoA's role in facilitating the

thermodynamic-linkage observed between pyruvate and MgATP. We aim to determine exactly which CT and BC domains within the tetramer are communicating within a given catalytic cycle through a method of directed rehybridization of monomers, which utilizes irreversible cysteine residue crosslinkers bismaleimidoethane (BMOE) and bismaleimidohexane (BMH) to link dilute monomers at their allosteric domains. Residues Asp1043 and Gly1069 have been chosen based on their locations at the surface of the enzyme, mutated to cysteines *via* site-directed mutagenesis, and confirmed through sequence verification. From there, we will be able to perform steady-state kinetic analysis of different combinations of the rehybridized tetramers and compare their rates of pyruvate carboxylation and pyruvate-stimulated P_i release. Additionally, these experiments will allow us to determine whether PC's mechanism involves obligatory oscillating catalysis, which would provide kinetic evidence to support the symmetric and asymmetric PC structures elucidated by other lab groups (12, 14, 24).

REFERENCES

1. Jitrapakdee, S., and Wallace, J. (1999) Structure, Function, and Regulation of Pyruvate Carboxylase. *Biochem. J.* **340**, 1-16

2. Jitrapakdee, S., St. Maurice, M., Rayment, I., Cleland, W.W., Wallace, J.C., and Attwood, P.V. (2008) Structure, Mechanism and Regulation of Pyruvate Carboxylase. *Biochem. J.* **413**, 369-387

3. Jitrapakdee, S., Vidal-Puig, A., and Wallace, J.C. (2006) Anaplerotic Roles of Pyruvate Carboxylase in Mammalian Tissues. *Cell. Mol. Life. Sci.* **63**, 843-854

4. Adina-Zada, A., Zeczycki, T.N., and Attwood, P.V. (2012) Regulation of the structure and activity of pyruvate carboxylase by acetyl CoA. *Arch. Biochem. Biophys.* **519**, 118-130

5. Lietzan, A. D., and St. Maurice, M. (2013) A Substrate-Induced Biotin Binding Pocket in the Carboxyltransferase Domain of Pyruvate Carboxylase. *J. Biol. Chem.* **288**, 19915-19925

6. Zeczycki, T. N., Menefee, A.L., Adina-Zada, A., Jitrapakdee, S., Surinya, K.H., Wallace, J.C., Attwood, P.V., St. Maurice, M., and Cleland, W.W. (2011) Novel Insights into the Biotin Carboxylase Domain Reactions of Pyruvate Carboxylase from Rhizobium etli. *Biochemistry* **50**, 9724-9737

7. Zeczycki, T. N., St. Maurice, M., Jitrapakdee, S., Wallace, J.C., Attwood, P.V., and Cleland, W.W. (2009) Insight into the Carboxyl Transferase Domain Mechanism of Pyruvate Carboxylase from Rhizobium etli. *Biochemistry* **48**, 4305-4313

8. St. Maurice, M., Reinhardt, L., Surinya, K.H., Attwood, P.V., Wallace, J.C., Cleland, W.W., and Rayment, I. (2007) Domain Architecture of Pyruvate Carboxylase, a Biotin-Dependent Multifunctional Enzyme. *Science* **317**, 1076-1079

9. Broussard, T., Pakhomova, S., Neau, D.B., Bonnot, R., and Waldrop, G.L. (2015) Structural Analysis of Substrate, Reaction Intermediate and Product Binding in Haemophilus influenzae Biotin Carboxylase. *Biochemistry* **54**, 3860-3870

10. Tong, L. (2013) Structure and Function of Biotin-Dependent Carboxylases. *Cell Mol. Life Sci.* **70**, 863-891

11. Zeczycki, T. N., Menefee, A.L., Jitrapakdee, S., Wallace, J.C., Attwood, P.V., St. Maurice, M., and Cleland, W.W. (2011) Activation and Inhibition of Pyruvate Carboxylase from Rhizobium etli. *Biochemistry* **50**, 9694-9707

12. Yu, L. P. C., Xiang, S., Lasso, G., Gil, D. Valle, M., and Tong, L. (2009) A Symmetrical Tetramer for S. aureus Pyruvate Carboxylase in Complex with Coenzyme A. *Structure* **17**, 823-832

13. Lietzan, A. D., Menefee, A.L., Zeczycki, T.N., Kumar, S., Attwood, P.V., Wallace, J.C., Cleland, W.W., and St. Maurice, M. (2011) Interaction Between the Biotin Carboxyl Carrier Domain and the Biotin Carboxylase Domain in Pyruvate Carboxylase from Rhizobium etli. *Biochemistry* **50**, 9708-9723

14. Lasso, G., Yu, L.P.C., Gil, D., Lázaro, M., Tong, L., and Valle, M. (2014) Functional Conformations for Pyruvate Carboxylase during Catalysis Explored by Cryoelectron Microscopy. *Structure* **22**, 911-922

15. Xiang, S., and Tong, L. (2008) Crystal Structures of Human and Staphylococcus aureus Pyruvate Carboxylase and Molecular Insights into the Carboxyltransfer Reaction. *Nat. Struct. Mol. Bio.* **15**, 295-302

16. Duangpan, S., Jitrapakdee, S., Adina-Zada, A., Byrne, L., Zeczycki, T.N., St. Maurice, M., Cleland, W.W., Wallace, J.C., and Attwood, P.V. (2010) Probing the Catalytic Roles of Arg548 and Gln552 in the Carboxyl Transferase Domain of the Rhizobium etli Pyruvate Carboxylase by Site-Directed Mutagenesis. *Biochemistry* **49**, 3296-3304

17. Samuel, V. T., and Shulman, G.I. (2016) The Pathogenesis of Insulin Resistance: Integrating Signaling Pathways and Substrate Flux. *J. Clin. Invest.* **126**, 12-22

18. Boden, G. (1997) Role of Fatty Acids in the Pathogenesis of Insulin Resistance and NIDDM. *Diabetes* **46**, 3-10

19. Perry, R. J., Camporez, J.G., Kursawe, R., Titchenell, P.M., Zhang, D., Perry, C.J., Jurczak, M.J., Abudukadier, A., Han, M.S., Zhang, X., Ruan, H., Yang, X., Caprio, S., Kaech, S.M., Sul, H.S., Birnbaum, M.J., Davis, R.J., Cline, G.W., Petersen, K.F., and Shulman, G.I. (2015) Hepatic Acetyl CoA Links Adipose Tissue Inflammation to Hepatic Insulin Resistance and Type 2 Diabetes. *Cell* **160**, 745-758

20. Khew-Goodall, Y. S., Johannssen, W., Attwood, P.V., Wallace, J.C., and Keech, D.B. (1991) Studies on Dilution Inactivation of Sheep Liver Pyruvate Carboxylase. *Arch. Biochem. Biophys.* **284**, 98-105

21. Goodey, N. M., and Benkovic, S.J. (2008) Allosteric regulation and catalysis emerge via a common route. *Nature Chem. Biol.* **4**, 474-482

22. Goodall, G. J., Baldwin, G.S., Wallace, J.C., and Keech, D.B. (1981) Factors that influence the translocation of the N-carboxybiotin moiety between the two sub-sites of pyruvate carboxylase. *Biochem. J.* **199**, 603-609

23. Warren, G. B., and Tipton, K.F. (1974) Pig Liver Pyruvate Carboxylase. The Reaction Pathway for the Decarboxylation of Oxaloacetate. *Biochem. J.* **139**, 321-329

24. Lasso, G., Yu, L.P.C., Gil, D., Xiang, S., Tong, L., and Valle, M. (2010) Cryo-EM Analysis Reveals New Insights into the Mechanism of Action of Pyruvate Carboxylase. *Structure* **18**, 1300-1310

25. Upson, R. H., Malekzadeh, M.N., and Haughland, R.P. (1996) A Spectrophotometric Method to Measure Enzymatic Activity in Reactions that Generate Inorganic Pyrophosphate. *Anal. Biochem.* **243**, 41-45

26. Webb, M. R. (1992) A Continuous Spectrophotometric Assay for Inorganic Phosphate and for Measuring Phosphate Release Kinetics in Biological Systems. *Proc. Nat. Acad. Sci.* **89**, 4884-4887

27. Attwood, P. V., Wallace, J.C., and Keech. D.B. (1984) The Carboxybiotin Complex of Pyruvate Carboxylase. A Kinetic Analysis of the Effects of Mg2+ Ions on its Stability and on its Reaction with Pyruvate. *Biochem. J.* **219**, 243-251

28. Easterbrook-Smith, S. B., Wallace, J.C., and Keech, D.B. (1978) A Reappraisal of the Reaction Pathway of Pyruvate Carboxylase. *Biochem. J.* **169**, 225-228

29. Reinhart, G. D. (2004) Quantitative Analysis and Interpretation of Allosteric Behavior. In *Methods in Enzymology* (Press, A., ed) Vol. 380. Energetics of Biological Macromolecules, Part E pp. 187-203, Elsevier

30. Monod, J., Wyman, J., and Changeaux, J.P. (1965) On the Nature of Allosteric Transitions: A Plausible Model. *J. Mol. Biol.* **12**, 88-118

31. Weber, G. (1972) Ligand Binding and Internal Equilibria in Proteins. *Biochemistry* **11**, 864-878

32. Wyman, J. (1967) Allosteric Linkage. *J. Am. Chem. Soc.* **89**, 2202-2218

33. Fenton, A. W., Paricharttanakul, N.M., and Reinhart, G.D. (2004) Disentangling the Web of Allosteric Communication in a Homotetramer: Heterotropic Activation in Phosphofructokinase from Escherichia coli. *Biochemistry* **43**, 14104-14110

34. Fenton, A. W. (2008) Allostery: an illustrated definition for the 'second secret of life'. *Trends Biochem. Sci.* **33**, 420-425

35. Adina-Zada, A., Zeczycki, T.N., St. Maurice, M., Jitrapakdee, S., Cleland, W.W., and Attwood, P.V. (2012) Allosteric regulation of the biotin-dependent enzyme pyruvate carboxylase by acetyl-CoA. *Biochem. Soc. Trans.* **40**, 567-572

36. Barden, R. E., Fung, C.H., Utter, M.F., and Scrutton, M.C. (1972) Pyruvate Carboxylase from Chicken Liver: Steady State Kinetic Studies Indicate a "Two-Site" Ping-Pong Mechanism. *J. Biol. Chem.* **247**, 1323-1333

37. Cleland, W. W. (1963) The kinetics of enzyme-catalyzed reactions with two or more substrates or products: I. Nomenclature and rate equations. *Biochim. Biophys. Acta* **67**, 104-137

38. Sheely, M. L. (1932) Glycerol Viscosity Tables. *Ind. Eng. Chem.* **24**, 1060-1064

39. Swindells, J. F., Snyder, C.F., Hardy, R.C., and Golden, P.E. (1958) Viscosities of Sucrose Solutions at Various Temperatures: Tables of Recalculated Values. *U.S. Dept. of Commerce National Bureau of Standards* **Circular 440**, 1-7

40. Telis, V. R. N., Telis-Romero, J., Mazzotti, H.B., and Gabas, A.L. (2007) Viscosity of Aqueous Carbohydrate Solutions at Different Temperatures and Concentrations. *Int. J. Food Props.* **10**, 185-195

41. Rickwood, D., and Birnie, G.D. (1974) Metrizamide, a New Density-Gradient Medium. *FEBS Letters* **50**, 102-110

42. Rashid, R., Chee, S.M.L., Raghunath, M., and Wohland, T. (2015) Macromolecular Crowding Gives Rise to Microviscosity, Anomalous Diffusion, and Accelerated Actin Polymerization. *Phys. Biol.* **12**, 1-7

43. Mastro, A. M., Babich, M.A., Taylor, W.D., and Keith, A.D. (1984) Diffusion of a Small Molecule in the Cytoplasm of Mammalian Cells. *Proc. Nat. Acad. Sci.* **81**, 3414-3418

44. Luby-Phelps, K. (1999) Cytoarchitecture and Physical Properties of Cytoplasm: Volume, Viscosity, Diffusion, Intracellular Surface Area. *Int. Rev. Cytology* **192**, 189-221

45. Bicknese, S., Periasamy, N., Shohet, S.B., and Verkman, A.S. (1993) Cytoplasmic viscosity near the cell plasma membrane: measurement by evanescent field frequency-domain microfluorimetry. *Biophys. J.* **65**, 1272-1282